



# Synthesis, Characterization, DFT Studies and Biological Activity of Ru(III), La(III) and Ce(III) Triphenylphosphine Complexes Containing 2-Aminothiazole and 2-Aminotriazole

Satish Naik<sup>1</sup> · P. Parameshwara Naik<sup>1</sup> · G. Krishnamurthy<sup>1</sup> · N. Venugopal<sup>1</sup> · Nagaraja Naik<sup>2</sup> · T. R. Ravikumar Naik<sup>3</sup>

Received: 9 December 2019 / Accepted: 3 March 2020 / Published online: 19 March 2020  
© Springer Science+Business Media, LLC, part of Springer Nature 2020

## Abstract

In the present paper a series of triphenylphosphine complexes containing mixed ligands like 2-aminothiazole (Ath) and 2-aminotriazole (Atz) have been prepared. The complexes are of the formula  $[MCl_3((Pph_3)(Ath)_2)]$  and  $[MCl_3((Pph_3)(Atz)_2)]$ ,  $[M = Ru(III), Ce(III) \text{ and } La(III)]$ . These complexes were characterized by different spectral techniques. Additionally, the computational study has been performed using density functional theory (DFT) and the calculation is used to examine the electronic structure of the synthesized complexes. The biological activities of all the synthesized complexes were evaluated and the comparative account in properties between the triphenylphosphine metal complexes containing 2-aminothiazole and 2-aminotriazole ligands has been made. The DNA-binding property of these metal complexes was investigated using electronic absorption spectroscopy and fluorescence spectroscopy. The antibacterial and antifungal activity against bacterial species (Gram –ve bacteria: *Escherichia coli*, *Salmonella typhi*) and (Gram +ve bacteria: *Staphylococcus aureus* and *Bacillus subtilis*) and fungi (*Aspergillus niger* and *Candida albicans*). The antioxidant study was carried out against the 2,2-diphenyl-1-picrylhydrazyl radical (DPPH) which showed that the metal complexes are good antioxidant, as compared to BHT. Further, the in-silico molecular docking study was performed to predict the possible binding sites of the metal complexes.

**Keywords** DFT · DNA binding · Antioxidant · Molecular docking

## 1 Introduction

A series of mixed ligand complexes  $Ln(Pip)_3(Phen)$  ( $Ln(III) = La, Ce-Nd, Sm-Lu, Y$ ; HPip (CAPH type ligand) = 2,2,2-trichloro-*N*-(dipiperidin-1-yl-phosphoryl)acetamide, Phen = 1,10-phenanthroline) has been synthesized. The newly formed metal complexes are structurally characterized by different spectroscopic techniques [1]. Lanthanum(III) tris (o-tolyl/benzyl)dithio-carbonates),  $[La(ROCS_2)]$

( $R = o-, m-, p-CH_3C_6H_4$  and  $C_6H_5CH_2$ ) were isolated as yellow solid by the reaction of  $LaCl_3 \cdot 7H_2O$  with sodium salt of tolyl/benzyl-di-thiocarbonates,  $ROCS_2Na$  ( $R = o-, m-, p-CH_3C_6H_4$  and  $C_6H_5CH_2$ ) in methanol under anhydrous conditions in 1:3 molar ratio. These complexes have formed adducts with nitrogen and phosphorus donor molecules by straight forward reaction of these complexes [2]. Lanthanum complexes were also obtained with a diimine ligand in three different redox states [3]. Some lanthanum(III) complexes have been synthesized by reacting lanthanum(III) metal salt with Schiff bases derived from 3-substituted-4-amino-5-mercapto-1,2,4-triazole (L) and glyoxal/biacetyl/benzyl. All these complexes were not soluble in common organic solvents but sparingly soluble in DMF and DMSO. The chelation of the complexes has been proposed in the light of analytical and spectral studies [4].

A number of cerium alkoxides were synthesized from the reaction of  $Ce\{N[Si(CH_3)_3]_2\}_3$  and the appropriate alcohol: neopentyl alcohol  $[H-OCH_2C(CH_3)_3-H-ONep]$ , tert-butyl alcohol  $[H-OC(CH_3)_3-H-OtBu]$  or 2,6-diphenylphenol using toluene, tetrahydrofuran (THF) or pyridine (py). Once isolated, several of these species were further

✉ P. Parameshwara Naik  
parashchem@gmail.com

✉ G. Krishnamurthy  
gkmaikshahyadri@gmail.com

<sup>1</sup> Department of Chemistry, Sahyadri Science College, Kuvempu University, Shivamogga, Karnataka 577201, India

<sup>2</sup> Department of Studies in Chemistry, University of Mysore, Manasagangotri, Mysore, Karnataka 06, India

<sup>3</sup> Veerasaiva Vidyavardhaka College, Ballari, Karnataka 583101, India

reacted with a series of sterically varied carboxylic acid modifiers including isobutyric acid [ $\text{H}-\text{O}_2\text{CCH}(\text{CH}_3)_2=\text{H}-\text{OPc}$ ] and trimethylacetic acid [ $\text{H}-\text{O}_2\text{CC}(\text{CH}_3)_3=\text{H}-\text{OBc}$ ] [5].

Many mixed-ligand complexes containing chelating  $\beta$ -diketonate ligands have been successfully employed as molecular precursors for the MOCVD (metal–organic chemical vapour deposition) production of pure  $\text{CeO}_2$  and yttria-doped  $\text{CeO}_2$  thin films due to their relatively high volatility [6–8].  $\text{Ce}(\text{Pc})_2$  is a sandwich complex in which the cerium atom is 8-coordinated by the isoindole nitrogens of the two staggered convex Pc-rings [9, 10].

A novel method was developed for preparing a series of trans nitrosyl complexes of general formula  $\text{trans}[\text{Ru}(\text{NH}_3)_4\text{L}(\text{NO})](\text{BF}_4)_3$ , where L = imidazole, L-histidine, pyridine, or nicotinamide [11].

Quantum chemical calculations at the DFT level have been carried out to analyze quantitatively the  $\text{Ru}^{\text{II}}-(\text{NO})^+$ ,  $\text{Ru}^{\text{III}}-(\text{NO})^0$  and  $\text{Ru}^{\text{II}}-(\text{NO})^0$  bonds in  $\text{trans}[\text{Ru}^{\text{II}}(\text{NH}_3)_4(\text{L})(\text{NO})]^q$  and  $\text{trans}[\text{Ru}^{\text{II}}(\text{NH}_3)_4(\text{L})(\text{NO})]^{q-1}$  complexes, where L = 4-picoline (4-pic), C-bound imidazole (imC), N-bound imidazole (imN), nicotinamide (nic), pyridine (py) and pyrazine (pz). Equilibrium geometries and the vibrational frequencies are reported for the ground state (GS) and light-induced metastable states,  $\text{MS}_1$  and  $\text{MS}_2$  presenting good agreement with the experimental data. The nature of the  $\text{Ru}^{\text{II}}-(\text{NO})^+$  and  $\text{Ru}^{\text{II}}-(\text{NO})^0$  bonds was investigated by means of the energy decomposition analysis (EDA) [12, 13].

In the view of the above, herewith we report synthesis of complexes of Ru(III), La(III) and Ce(III) triphenyl phosphine compounds with Ath and Atz ligands. In this paper the structure and biological activity of the above complexes have also been compared.

## 2 Experimental

### 2.1 Reagents and Physical Measurements

All the reagents needed for the present work were commercially available, analytical grade and obtained from Sigma Aldrich, Merck and Hi Media Ltd., utilized without further purification. Microanalytical data (Carbon, Hydrogen and Nitrogen) was carried out on Vario EL CHNOS elemental analyser. The electronic spectra of the compounds were recorded on Shimadzu model 1650 UV–Visible double beam spectrometer in the range of 200–800 nm in DMF solution ( $10^{-3}$  M). FTIR spectra studies were carried out using KBr discs on a Bruker alpha-T FTIR Spectrophotometer in the range of 4000–400  $\text{cm}^{-1}$ . The conductivity measurement of the metal complexes was determined in ( $10^{-3}$  M) DMF solution using an ELICO-CM82 conductivity bridge. The magnetic moment values of the complexes were calculated at room temperature on a Gouy balance model 7550 applying  $\text{Hg}[\text{Co}(\text{NCS})_4]$  as a calibrant.

### 2.2 Synthesis of $[\text{Ru}(\text{Pph}_3)(\text{Ath})_2\text{Cl}_3]$

To the ethanolic solution of  $\text{RuCl}_3$  (0.5 g, 3.6 mmol), the solution of triphenylphosphine (0.94 g, 3.6 mmol) in ethanol was mixed and stirred at reflux for 10 min. To the above solution, the hot ethanolic solution of the 2-aminothiazole (0.36 g, 3.6 mmol) was added. The mixture was refluxed with stirring for 6 h; the solid so precipitated after evaporation of excess solvent to dryness was collected and was dried under vacuum to get dark-green/block coloured solid. The solid product was recrystallized from the methanol and the obtained complex was kept in a vacuum desiccator. The melting point of the product was  $> 300$  °C. Yield: 69%. The physical properties and the analytical data is given in Table 1, MS ( $\text{C}_{21}\text{H}_{19}\text{Cl}_2\text{RuN}_2\text{PS}$ ) = 498.72 g/mol. The proposed structure of the complexes is shown in Fig. 1.

### 2.3 Synthesis of $[\text{Ru}(\text{Pph}_3)(\text{Atz})_2\text{Cl}_3]$

To synthesize this complex, the procedure given above was followed excepting the addition of 2-aminotriazole (0.36 g, 3.6 mmol) in ethanol rather than 2-aminothiazole. The dark green colored product left out after the evaporation of excess solvent. Yield: 69%. The physical properties and the analytical data is given in Table 1, MS ( $\text{C}_{21}\text{H}_{19}\text{Cl}_2\text{RuN}_2\text{PS}$ ) = 498.72 g/mol.

### 2.4 Synthesis of $[\text{La}(\text{Pph}_3)(\text{Ath})_2\text{Cl}_3]$

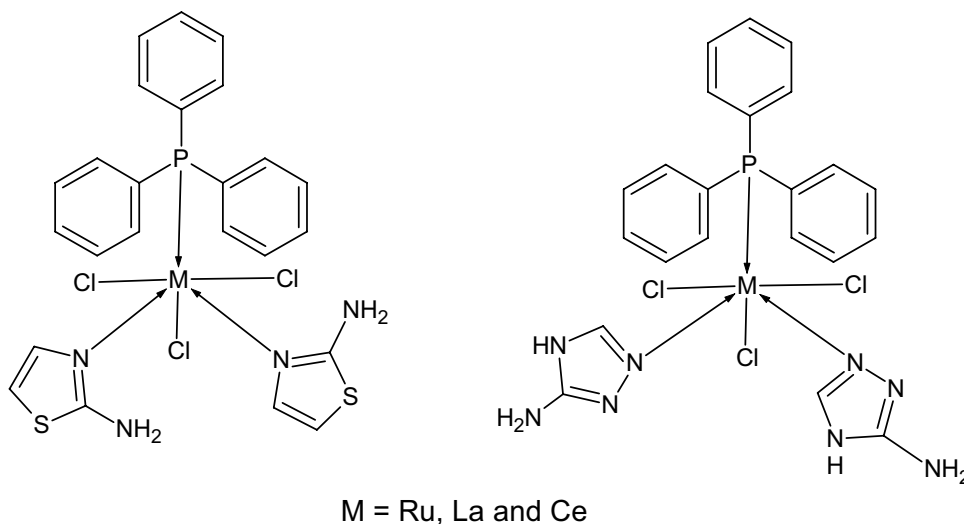
The ethanolic solution of triphenylphosphine (0.94 g, 3.6 mmol) was added to the ethanolic solution of  $\text{LaCl}_3$  (0.5 g, 3.6 mmol) and the solution was stirred with heating for about 10 min. To the above solution, a hot ethanolic solution of the 2-aminothiazole (0.36 g, 3.6 mmol) was added and the resulting solution was refluxed with stirring on a magnetic stirrer with hot-plate fitted with water cooled condenser for about 4–5 h. The solid is precipitated on evaporating the excess of ethanol to dryness under vacuum to give yellow coloured solid. The solid product was recrystallized from the methanol and the obtained complex was kept in a vacuum desiccator. Yield: 69%. The physical properties and the analytical data are given in Table 1. MS ( $\text{C}_{21}\text{H}_{19}\text{Cl}_3\text{LaN}_2\text{PS}$ ) = 498.72 g/mol. LC–MS (positive): m/z 499.02.

### 2.5 Synthesis of $[\text{La}(\text{Pph}_3)(\text{Atz})_2\text{Cl}_3]$

The procedure given above was followed to synthesize this complex but, excepting addition of the solution of 2-aminothiazole ligand (0.36 g, 3.6 mmol) in ethanol, 2-aminotriazole was added. The colour of the product is straw-yellow.

**Table 1** Physical and analytical data of the synthesized complexes

Compound	C	H	N	S	Cl	Conductance ( $\text{Ohm}^{-1}$ $\text{cm}^2 \text{mol}^{-1}$ )	Mol. Wt	M pt ( $^{\circ}\text{C}$ )
$[\text{RuCl}_3(\text{Pph}_3)(\text{Ath})_2]$	43.02 (42.98)	3.36 (3.28)	8.36 (8.28)	9.57 (9.51)	15.87 (15.77)	5.4	668.9	> 300
$[\text{RuCl}_3(\text{Pph}_3)(\text{Atz})_2]$	41.42 (40.93)	3.63 (3.05)	17.57 (16.91)	–	16.67 (17.21)	6.5	636.0	> 300
$[\text{LaCl}_3(\text{Pph}_3)(\text{Ath})_2]$	40.72 (40.68)	3.28 (3.22)	7.92 (7.89)	9.06 (9.00)	15.03 (15.00)	6.2	705.0	> 300
$[\text{LaCl}_3(\text{Pph}_3)(\text{Atz})_2]$	39.10 (40.87)	3.43 (2.99)	15.68 (16.79)	–	15.74 (16.13)	7.5	673.0	> 300
$[\text{CeCl}_3(\text{Pph}_3)(\text{Ath})_2]$	40.65 (40.61)	3.27 (3.21)	7.90 (7.88)	9.04 (9.00)	15.00 (14.95)	5.8	706.0	> 300
$[\text{CeCl}_3(\text{Pph}_3)(\text{Atz})_2]$	39.03 (38.99)	3.42 (3.39)	16.55 (16.49)	–	15.71 (15.69)	5.9	674.0	> 300

**Fig. 1** Proposed structure of the complexes

Yield: 69%. The physical properties and the analytical data are given in Table 1. MS ( $\text{C}_{21}\text{H}_{19}\text{Cl}_2\text{LaN}_2\text{PS}$ ) = 498.72 g/mol.

## 2.6 Synthesis of $[\text{Ce}(\text{Pph}_3)(\text{Ath})_2\text{Cl}_3]$

An ethanolic solution of  $\text{CeCl}_3$  (0.5 g, 3.6 mmol) was mixed with a hot stirring ethanolic solution of triphenylphosphine (0.94 g, 3.6 mmol) and the solution was stirred for about 10 min. The solution of 2-aminothiazole (0.36 g, 3.6 mmol) in ethanol was added to the above solution and stirring continued for about 4–5 h. The yellow coloured solid precipitated on evaporation of ethanol to dryness under vacuum. The solid product was recrystallized from the methanol and the obtained complex was kept in a vacuum desiccator. Colour of the product is pale-yellow and the melting point is > 300  $^{\circ}\text{C}$ . Yield: 69%. The physical properties and the analytical data are given in Table 1. MS

( $\text{C}_{21}\text{H}_{19}\text{Cl}_2\text{ZnN}_2\text{PS}$ ) = 498.72 g/mol. LC–MS (positive): m/z 499.02.

## 2.7 Synthesis of $[\text{Ce}(\text{Pph}_3)(\text{Atz})_2\text{Cl}_3]$

This complex was synthesized by following the procedure as discussed above except the addition of the solution of 2-aminotriazole ligand (0.36 g, 3.6 mmol) in ethanol rather than 2-aminothiazole was added. The melting point of the brown colored product was > 300  $^{\circ}\text{C}$ . Yield: 69%. The physical properties and the analytical data are given in Table 1. MS ( $\text{C}_{21}\text{H}_{19}\text{Cl}_2\text{CeN}_2\text{PS}$ ) = 498.72 g/mol.

## 2.8 DFT Studies

All computational calculations for the mixed ligand complexes were obtained using the Gaussian 09 software. The molecular geometry for synthesized compounds were

computed using density functional theory (DFT) based on Becke's three parameter hybrid exchange functional (B3LYP) and with LANL2DZ basis set. The optimized structure of the tested compounds has been visualized using chemcraft 1.7 software. Quantum chemical parameters such as ( $E_{\text{HOMO}}$ ), ( $E_{\text{LUMO}}$ ), energy gap ( $\Delta E$ ) and several other parameters were evaluated for the investigated molecule [14].

### 3 Biological Studies

#### 3.1 DNA Interaction Studies

The binding interaction between the metal ions and *CT*-DNA was investigated using UV–Vis spectroscopy. The required amount of DNA solution was prepared by dissolving in buffer medium (50 mM NaCl, 5 mM Tris–HCl and pH 7.2) UV absorbance value at 260 and 280 nm gave a ratio of about 1.8–1.9, revealing that the DNA is clear from the protein contamination. The concentration of *CT*-DNA per nucleotide was determined from its absorbance by employing a molar extinction coefficient value of 260 nm ( $\epsilon = 6600 \text{ M}^{-1} \text{ cm}^{-1}$ ) [15]. The metal complexes were dissolved in DMSO solvent because of low solubility in buffer solution. Absorption titration studies were carried with a fixed concentration of the complexes (10  $\mu\text{M}$ ) and by varying the concentration of DNA (0–50  $\mu\text{M}$ ). An equal volume of *CT*-DNA was added to the both complex solution and reference solution in order to remove the absorbance of *CT*-DNA itself. The intrinsic binding constant ( $K_b$ ) values of the complexes with DNA were measured by the following equation.

$$[\text{DNA}]/(\epsilon_a - \epsilon_f) = [\text{DNA}]/(\epsilon_b - \epsilon_f) + 1/K_b(\epsilon_b - \epsilon_f)$$

where [DNA] is the concentration of *CT*-DNA in base pairs,  $\epsilon_a$  is apparent coefficient of  $A_{\text{obsd}}/[\text{complex}]$ ,  $\epsilon_f$  and  $\epsilon_b$  correspond to the extinction coefficients of the free and fully bound forms of the complex respectively. A plot of  $[\text{DNA}]/(\epsilon_a - \epsilon_f)$  versus [DNA] gave a slope of  $1/(\epsilon_b - \epsilon_f)$  and Y-intercept equal to  $1/K_b(\epsilon_b - \epsilon_f)$ ,  $K_b$  is the ratio of slope to intercept.

#### 3.2 Fluorescence Quenching Studies

The experiment involving *CT* DNA was performed in 5 mM Tris–HCl/10 mM NaCl, pH 7.2 buffer solution. Tris–HCl buffer was prepared using doubly distilled water, followed by preparing of stock solution of *CT* DNA by dispersing the desired amount of *CT* DNA in the buffer solution. The resulting stock solution was stored at 4 °C and used within 4 days. To this metal complexes were added in successive additions. Then samples were

excited at 320 nm. The relative binding of the complexes to *CT*-DNA was determined by Stern–Volmer equation,  $I_0/I = 1 + KSVr$ , where  $I_0$  and  $I$  are the fluorescence intensities in the absence and presence of complexes respectively,  $KSV$  is a linear Stern–Volmer constant and  $r$  is the concentration [16].

#### 3.3 Antimicrobial Activity

The newly synthesized mixed ligand metal complexes were screened for their in vitro antimicrobial activity against two Gram-positive (*Staphylococcus aureus*, *Bacillus subtilis*) as well as two Gram-negative (*Escherichia coli*, *Salmonella typhi*) bacteria and two yeasts (*Aspergillus niger*, *Candida albicans*). Chloramphenicol and Fluconazole were used as standard antibacterial agent (control). The in-vitro antimicrobial activities of the newly synthesized compounds were examined by agar well diffusion method [17]. The test compounds had been dissolved in dimethylformamide to get a concentration of 0.5 and 1 mg/cm<sup>3</sup>. Sample poured petriplates were inoculated with microorganism and incubated at 37 °C for 24 h. DMF showed no inhibition zones. After incubation, the millimeter of inhibition zone around the well was measured. The minimum inhibitory concentration (MIC) value of the compounds was determined by serial dilution technique [18].

#### 3.4 Antioxidant Activity

The in-vitro radical scavenging activity of newly synthesized mixed ligand complexes against 2-diphenyl-1-picrylhydrazyl (DPPH) radical was determined by Blios method [19]. Different concentrations (50–100  $\mu\text{g}/\text{mL}$ ) of the tested compounds were used for examination. 1 mL aliquot of the test sample was added to 4 mL of a methanolic solution of DPPH and then the reaction mixture was incubated at 37 °C for 30 min in dark. After the completion of incubation time, the absorbance was taken at 517 nm and the percentage free radical scavenging % was calculated by the following equation. The butylated hydroxyl toluene (BHT) was used as positive control and all tests were conducted in triplicate.

$$\text{Scavenging ratio \%} = \left[ \frac{A_i - A_o}{A_c - A_o} \right] \times 100\%$$

where  $A_i$  is the absorbance in the presence of the test compound;  $A_o$  is absorbance of the blank in the absence of the test compound;  $A_c$  is the absorbance in the absence of the test compound.

#### 3.5 Molecular Docking

In-silico molecular docking studies were performed using HEX 6.1 software [20]. The structure of the synthesized mixed ligand complexes have been drawn by

CHEMSKETCH and saved to mol format by OPENBABEL (<https://www.vclab.org/lab/babel/>). The crystal structure of the Human Serum Albumin (PDB ID: 1h9z) was taken from the protein data bank (<https://www.rcsb.org/pdb>). All calculations were carried out on an Intel pentium4, 2.4 GHz based machine running MS Windows XP SP2 as operating system. The output results were analysed by ligplot and paymol software. The docking scores proved valuable information regarding the interaction of prepared compounds with active sites of the receptors.

## 4 Results and Discussion

The mixed ligand complexes were synthesised by following the literature as discussed in the experimental section. The physical properties and analytical data of the synthesized complexes are compiled in the Table 1. The molar conductance value of the complexes recorded in DMSO solvent at Ca.  $10^{-3}$  M. All the complexes are non-electrolytic in nature. A slight higher conductivity values for these complexes is due to partial dissociation of the complexes in solution and equilibrium may be established.

### 4.1 IR Spectral Studies

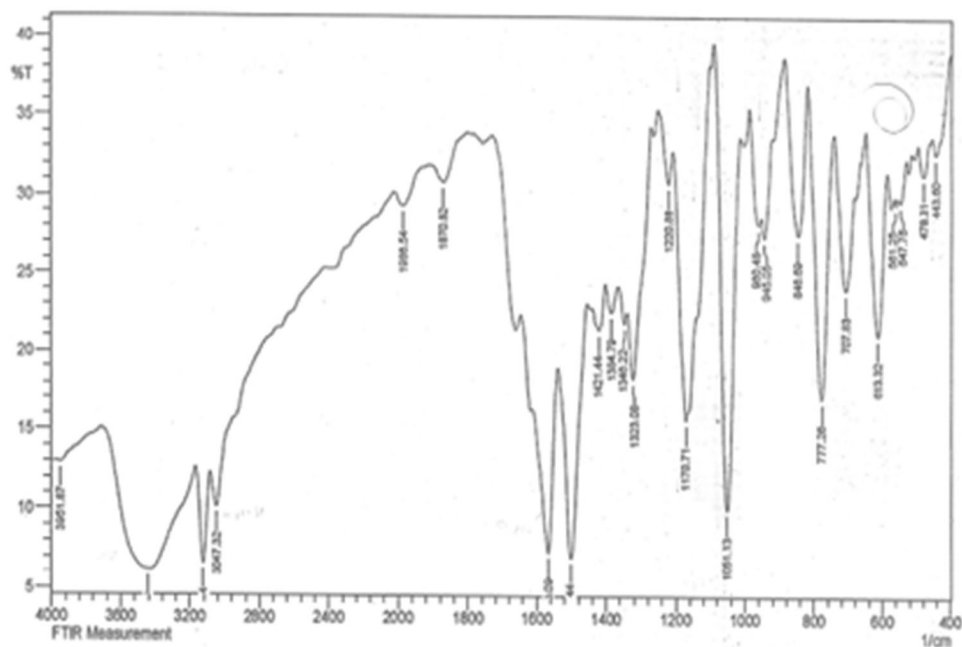
The IR spectra of the ligand and their complexes are recorded as KBr pellet. Infrared spectra of the ligands and their metal complexes are almost same except slight shift in the position of the peaks with different intensity confirms the coordination of ligand to metal ions. A sharp band

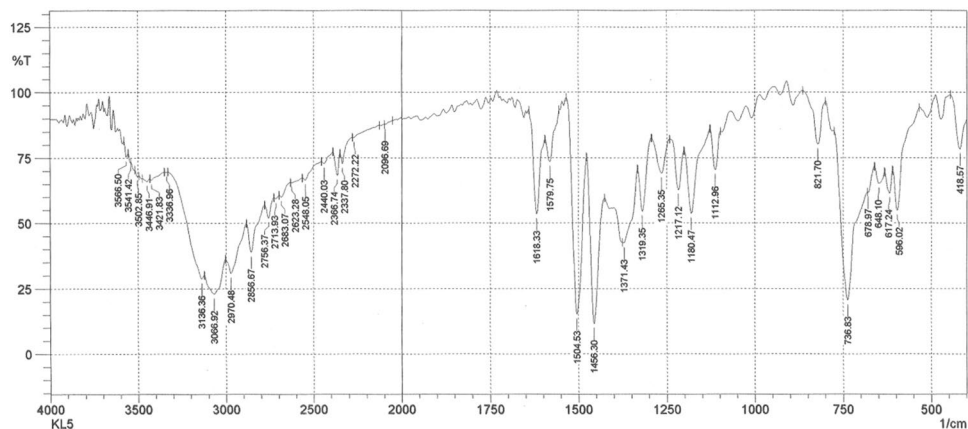
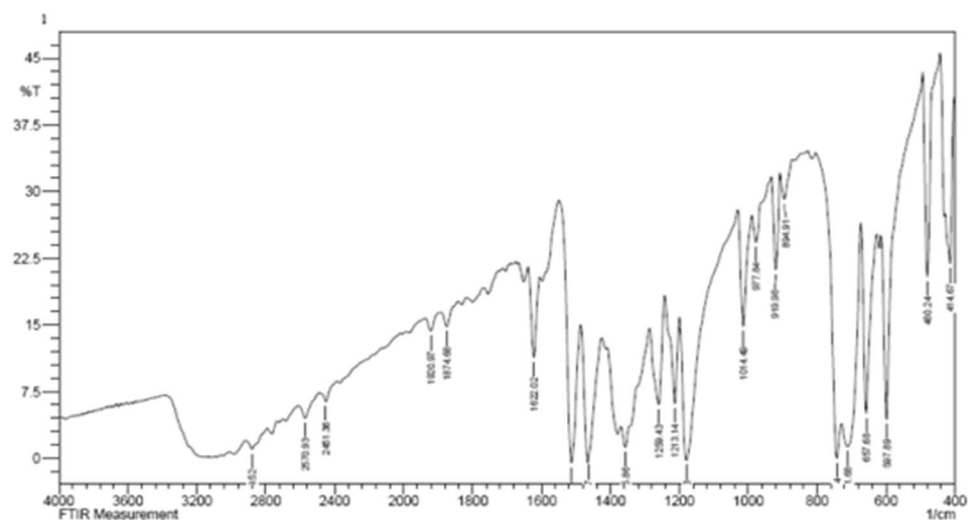
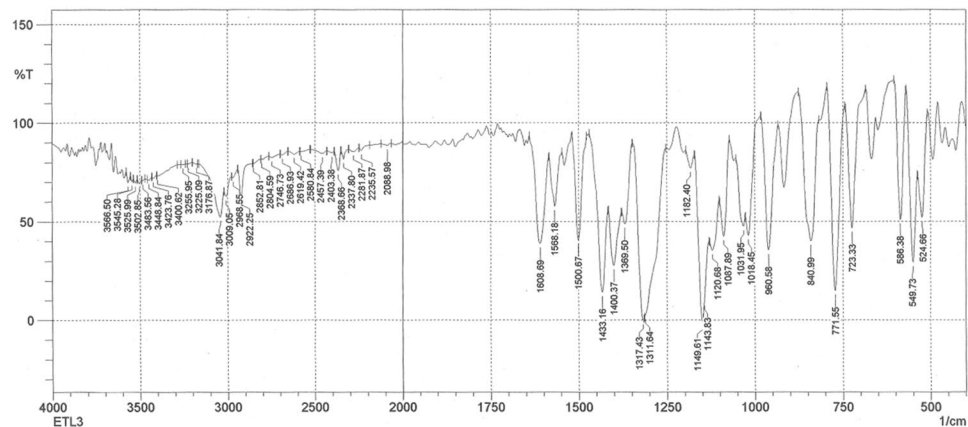
around  $3230\text{ cm}^{-1}$  was due to  $-\text{NH}_2$ . The band due to  $\text{C}=\text{N}$  stretching of ligand has been observed at lower frequency by  $20\text{--}30\text{ cm}^{-1}$  due to the formation metal complexes indicating the involvement of tertiary nitrogen in the coordination. The weak bands in the range  $540\text{--}650\text{ cm}^{-1}$  indicate  $\text{M}\text{--}\text{N}$  bond and a band in the region  $437\text{--}490\text{ cm}^{-1}$  is due to  $\text{M}\text{--}\text{Cl}$  stretching [20, 21]. The IR spectra of the mixed ligand metal complexes are showed in the Figs. 2, 3, 4, 5, 6, 7 and the values are compiled in Table 2.

### 4.2 UV-Absorption Spectral and Magnetic Susceptibility Studies

The electronic absorption spectra of heterocyclic mixed ligand Ru(III) complexes recorded in DMF within the range of  $900\text{--}200\text{ nm}$ , the band positions are showed in Figs. 8 and 9. The spectra showed four to five bands within the region  $15,748\text{--}36,101\text{ cm}^{-1}$ . Ruthenium(III) ground state is  $^2\text{T}_{2g}$  and the first excited doublet levels in the order of increasing energy are  $^2\text{A}_{2g}$  and  $^2\text{T}_{1g}$ , which arise from  $t_{2g}^4 e_g^1$  configuration [22]. The ligand Ath and Atz showed bands in the region ( $32,786\text{ cm}^{-1}$ )  $305\text{ nm}$  to ( $25,641\text{ cm}^{-1}$ )  $390\text{ nm}$  due to  $\pi \rightarrow \pi^*$  and  $n \rightarrow \pi^*$  transitions respectively of the aryl ring and the double bond of the  $>\text{C}=\text{N}-$  group [23, 24]. The electronic spectra of high spin  $[\text{RuCl}_3(\text{PPh}_3)(\text{Ath})_2]$  and  $[\text{RuCl}_3(\text{PPh}_3)(\text{Atz})_2]$  in which, the ruthenium(III) ion is in  $d^5$  electronic configuration has relatively high oxidizing properties and a large crystal field parameter and the charge transfer band of the type  $\text{L}\pi_y \rightarrow \text{T}_{2g}$  is noticeable in the low energy region, which obscures the weaker bands due to  $d\text{--}d$  transitions [25, 26]. In  $[\text{RuCl}_3(\text{PPh}_3)$

**Fig. 2** FT-IR spectrum of  $[\text{Ru}(\text{PPh}_3)(\text{Ath})_2\text{Cl}_3]$



**Fig. 3** FT-IR spectrum of  $[\text{Ru}(\text{Pph}_3)(\text{Atz})_2\text{Cl}_3]$ **Fig. 4** FT-IR spectrum of  $[\text{La}(\text{Pph}_3)(\text{Ath})_2\text{Cl}_3]$ **Fig. 5** FT-IR spectrum of  $[\text{La}(\text{Pph}_3)(\text{Atz})_2\text{Cl}_3]$ 

(Ath)<sub>2</sub>, the band at (20,830  $\text{cm}^{-1}$ ) 480 nm, (19,607  $\text{cm}^{-1}$ ) 510 nm, (17,090  $\text{cm}^{-1}$ ) 585 nm and (14,814  $\text{cm}^{-1}$ ) 675 nm due to  ${}^2\text{T}_{2g}(\text{F}) \rightarrow {}^4\text{T}_{1g}(\text{P})$  ( $\nu_3$ ),  ${}^2\text{T}_{2g}(\text{F}) \rightarrow {}^4\text{T}_{2g}(\text{F})$  ( $\nu_2$ ), and  ${}^2\text{T}_{2g} \rightarrow {}^4\text{A}_{2g}$  or  ${}^2\text{T}_{1g}(\nu_1)$  and  ${}^2\text{T}_{2g} \rightarrow {}^2\text{A}_{2g}$  transitions, which is in conformity with the assignments made for similar ruthenium(III) complexes [27]. Absorption in the region 19,343–25,576  $\text{cm}^{-1}$  displayed bands due to charge

transfer transitions. The design of the absorption spectra for the heterocyclic Ru(III) complexes confirm the proposed octahedral environment around the ruthenium(III) ion [17].  $[\text{RuCl}_3(\text{Pph}_3)(\text{Atz})_2]$  displayed four spin forbidden bands at (20,202  $\text{cm}^{-1}$ ) 495 nm, (19,047  $\text{cm}^{-1}$ ) 525 nm, (16,528  $\text{cm}^{-1}$ ) 605 nm and (14,814  $\text{cm}^{-1}$ ) 675 nm due to transition  ${}^2\text{T}_{2g}(\text{F}) \rightarrow {}^4\text{T}_{1g}(\text{P})$  ( $\nu_3$ ),  ${}^2\text{T}_{2g}(\text{F}) \rightarrow {}^4\text{T}_{2g}(\text{F})$  ( $\nu_2$ ),

**Fig. 6** FT-IR spectrum of  $[\text{Ce}(\text{Pph}_3)(\text{Ath})_2\text{Cl}_2]$

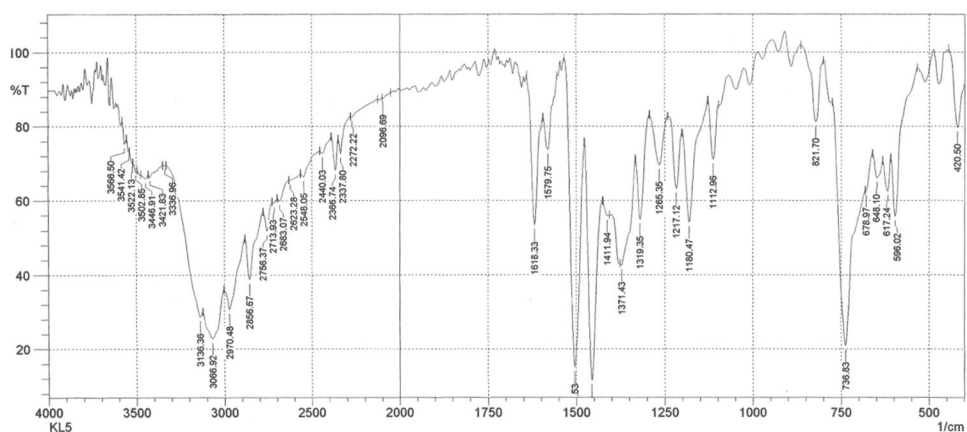


**Fig. 7** FT-IR spectrum of  $[\text{Ce}(\text{Pph}_3)(\text{Atz})_2\text{Cl}_3]$

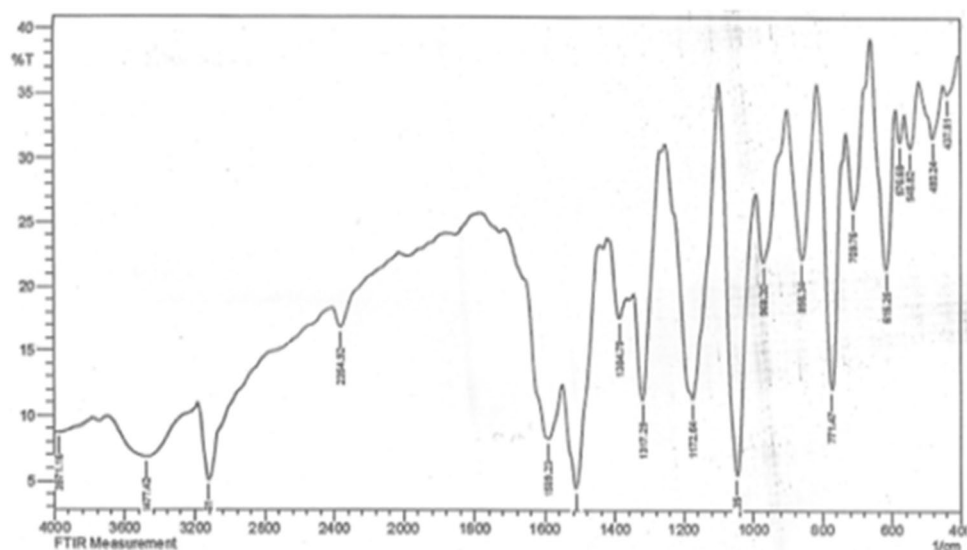


**Table 2** IR spectral data of the synthesized complexes ( $\text{cm}^{-1}$ )

Complex	N–H	C=N	M–P	M–N	M–Cl
$[\text{RuCl}_3(\text{Pph}_3)(\text{Ath})_2]$	3150	1510	845	650	450
$[\text{RuCl}_3(\text{Pph}_3)(\text{Atz})_2]$	3066	1579	821	607	445
$[\text{LaCl}_3(\text{Pph}_3)(\text{Ath})_2]$	3100	1555	841	597	440
$[\text{LaCl}_3(\text{Pph}_3)(\text{Atz})_2]$	4041	1506	840	549	445
$[\text{CeCl}_3(\text{Pph}_3)(\text{Ath})_2]$	3150	1500	850	600	490
$[\text{CeCl}_3(\text{Pph}_3)(\text{Atz})_2]$	3050	1539	836	540	437

and  ${}^2T_{2g} \rightarrow {}^4A_{2g}$  or  ${}^2T_{1g}(\nu_1)$ . The spectrum of the complex also displayed two bands, a high intensity band at ( $25,974 \text{ cm}^{-1}$ ) 385 nm is ascribed to symmetry forbidden ligand to metal charge transfer [23].

$[\text{CeCl}_3(\text{Pph}_3)(\text{Ath})_2]$  and  $[\text{CeCl}_3(\text{Pph}_3)(\text{Atz})]$  showed bands in the range of 402–468 nm, which may be assigned to ligand–metal charge transfer transitions Figs. 10 and 11. No

significant absorption in the visible region for lanthanide(III) complexes that may be due to the fact that the f–f bands are very weak and are obscured by the intense charge transfer bands that appear in this spectral region.

### 4.3 Magnetic Moment Studies

The magnetic moment value for the  $[\text{RuCl}_3(\text{Pph}_3)(\text{Atz})_2]$  and  $[\text{CeCl}_3(\text{Pph}_3)(\text{Atz})]$  complex was found to be 1.57 and 2.45 B.M respectively. The magnetic moment value for the  $[\text{RuCl}_3(\text{Pph}_3)(\text{Ath})_2]$  and  $[\text{CeCl}_3(\text{Pph}_3)(\text{Ath})_2]$  complex was found to be 1.76 and 2.43 B.M respectively. Slightly higher value in magnetic moment value for triazole complexes may be due strength of the ligand. These values suggest that all the complexes found to have octahedral geometry as proposed. The magnetic moment data show that the lanthanum(III) chloride complexes are diamagnetic in nature while all other complexes are paramagnetic as expected [28].

**Fig. 8** UV–Visible spectrum of  $[\text{RuCl}_3(\text{Pph}_3)(\text{Ath})_2]$

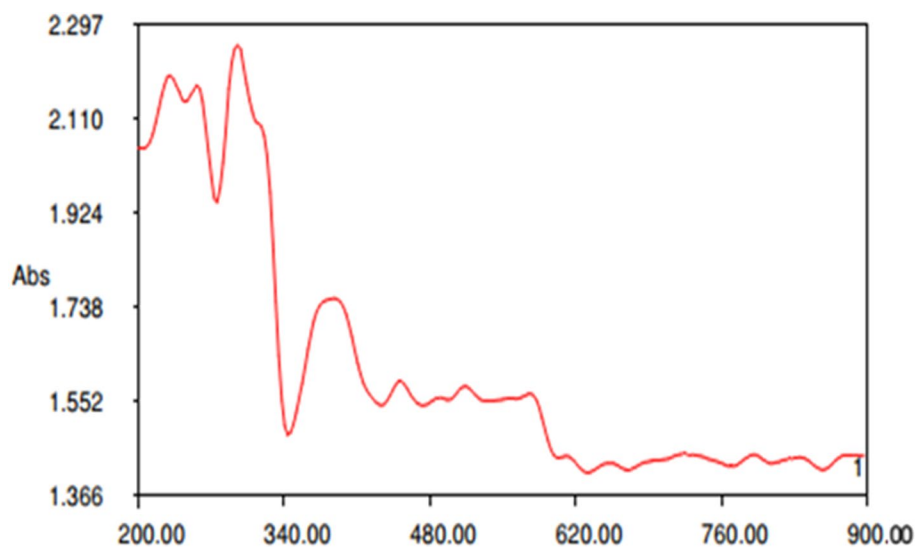


**Fig. 9** Electronic spectra of  $[\text{RuCl}_3(\text{Pph}_3)(\text{Atz})_2]$

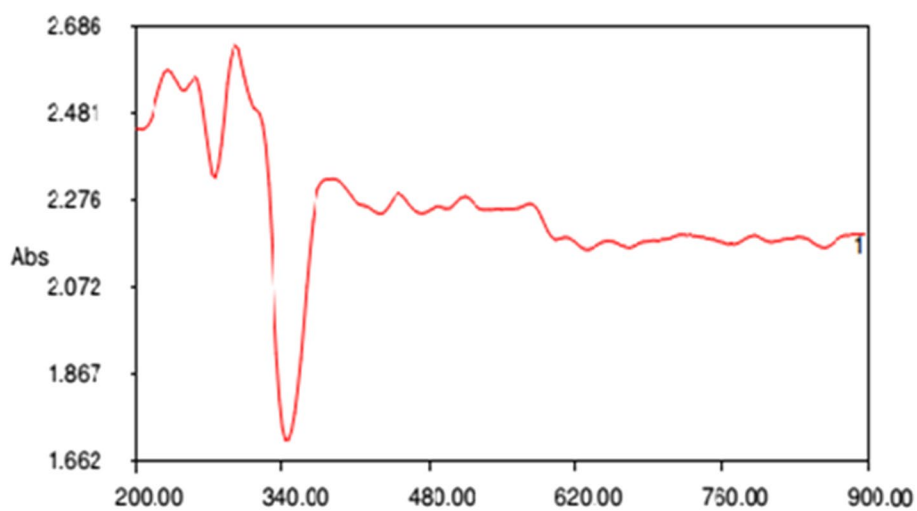


**Fig. 10** UV–Visible spectrum of  $[\text{CeCl}_3(\text{Pph}_3)(\text{Ath})_2]$

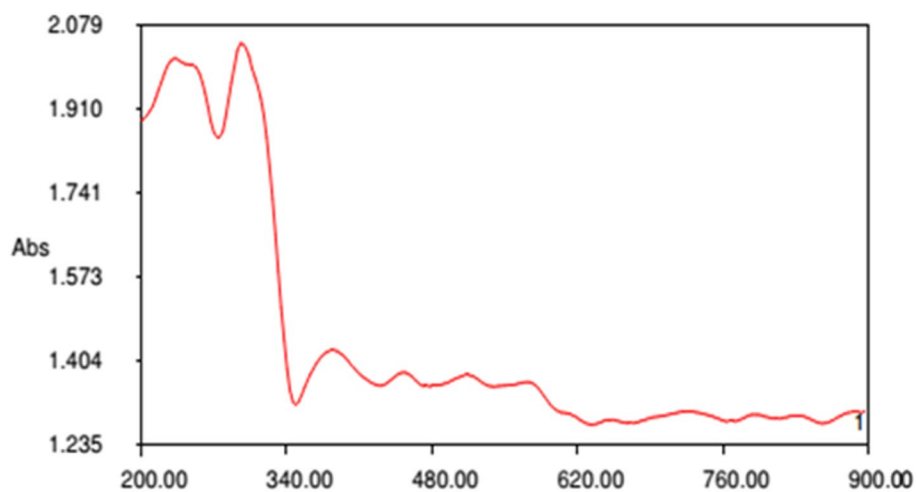




**Fig. 11** Electronic spectra of  $[\text{CeCl}_3(\text{PPh}_3)(\text{Atz})_2]$

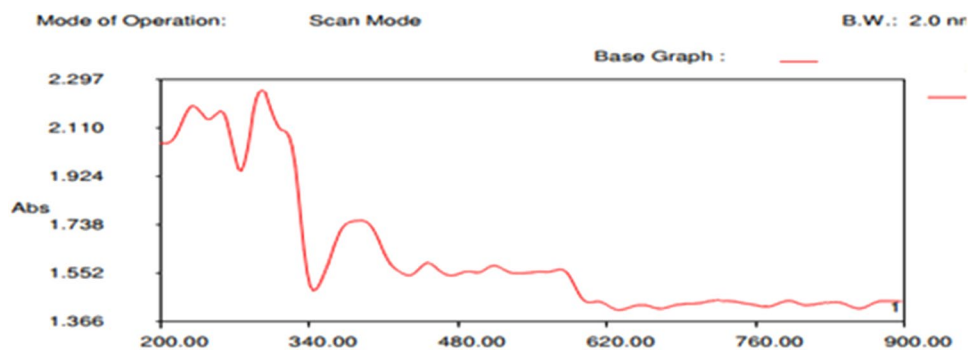


**Fig. 12** Mass spectrum of  $[\text{RuCl}_3(\text{PPh}_3)(\text{Ath})_2]$

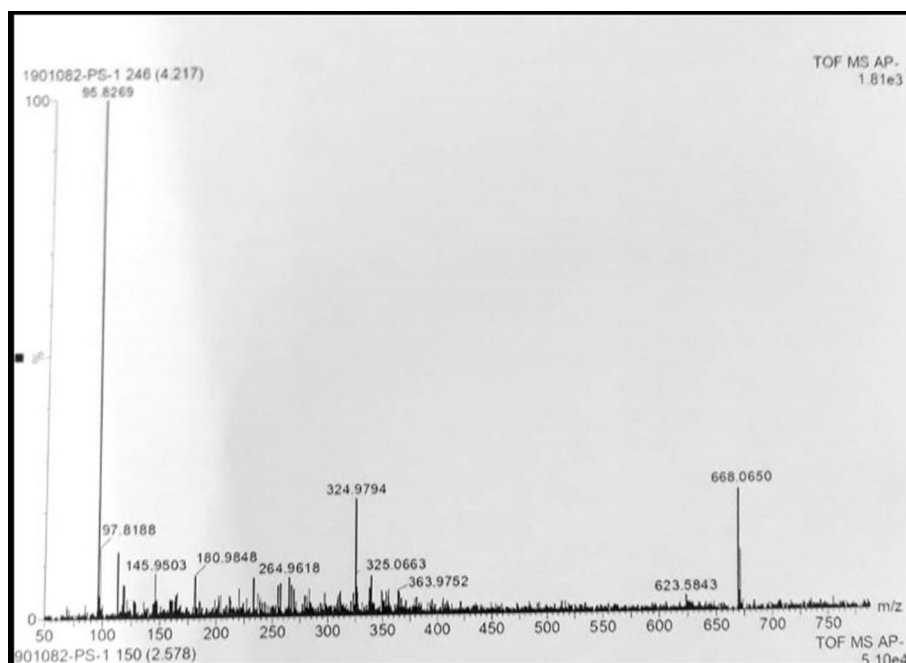


**Fig. 13** Optimised geometry and standard bond length of  $[\text{RuCl}_3(\text{PPh}_3)(\text{Ath})_2]$

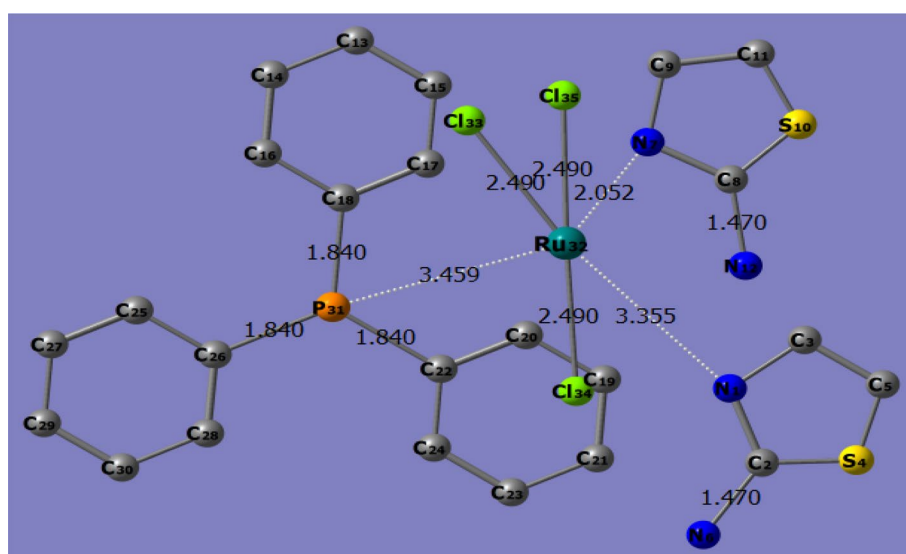


**Fig. 14** Optimised geometry and standard bond length of  $[\text{RuCl}_3(\text{Pph}_3)(\text{Atz})_2]$

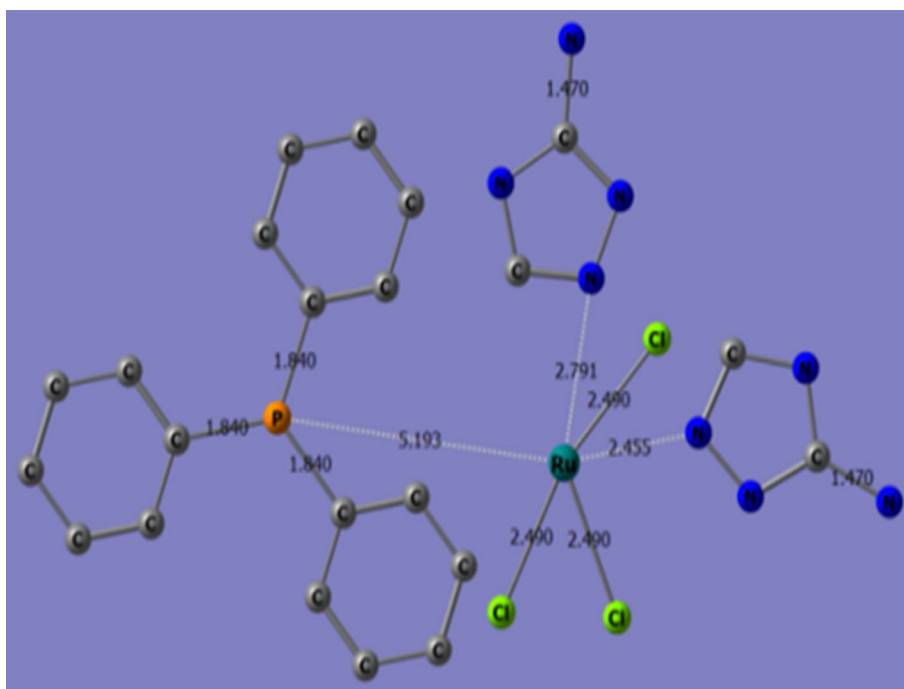
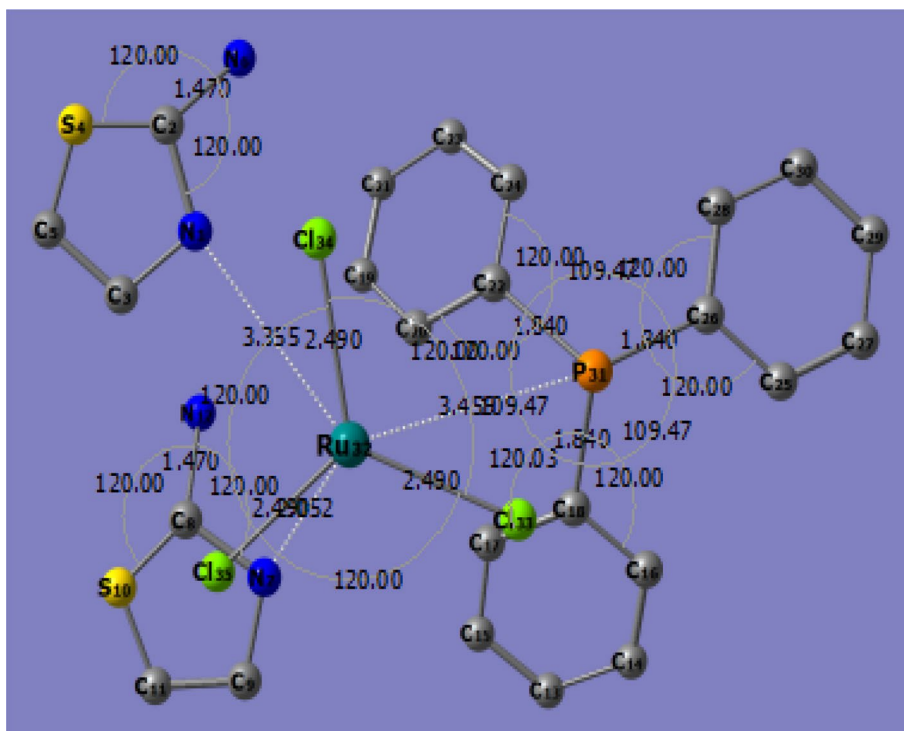


**Fig. 15** Standard bond angles of  $[\text{RuCl}_3(\text{Pph}_3)(\text{Ath})_2]$



#### 4.4 Mass Spectral Studies

The mass spectral study of  $[\text{RuCl}_3(\text{Pph}_3)(\text{Ath})_2]$  is recorded, which show a molecular ion peak at 668.06 is in good agreement with the calculated mass of the compound and showed in Fig. 12.

#### 5 DFT Studies of Complexes

The computational calculations of the complexes by Becke's three parameter hybrid exchange functional (B3LYP) with support of chemcraft 1.7 software [29, 30] has been used

**Fig. 16** Standard bond angles of  $[\text{RuCl}_3(\text{Pph}_3)(\text{Atz})_2]$

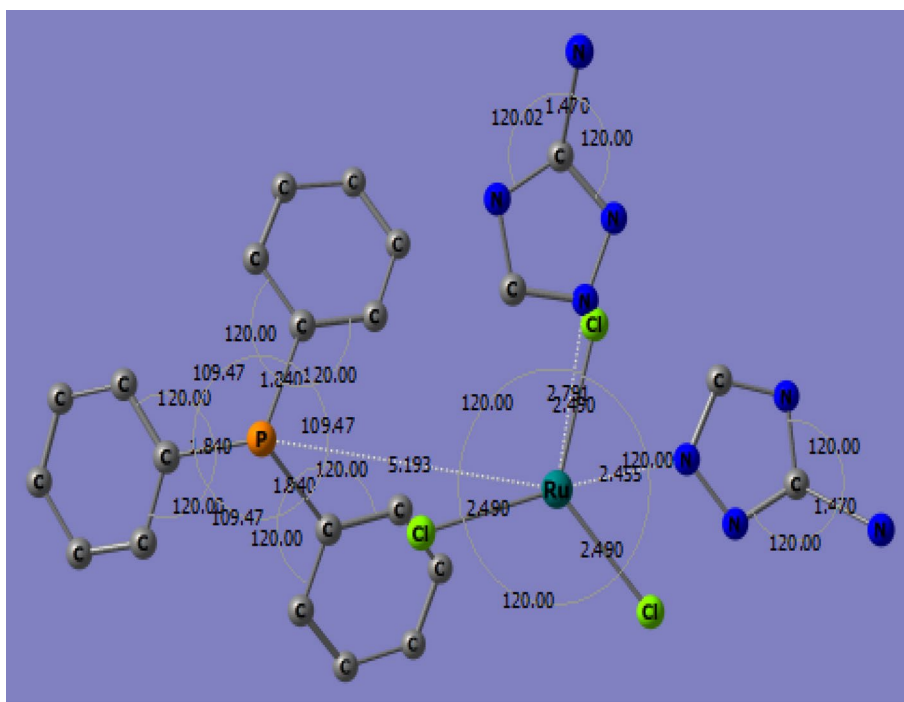
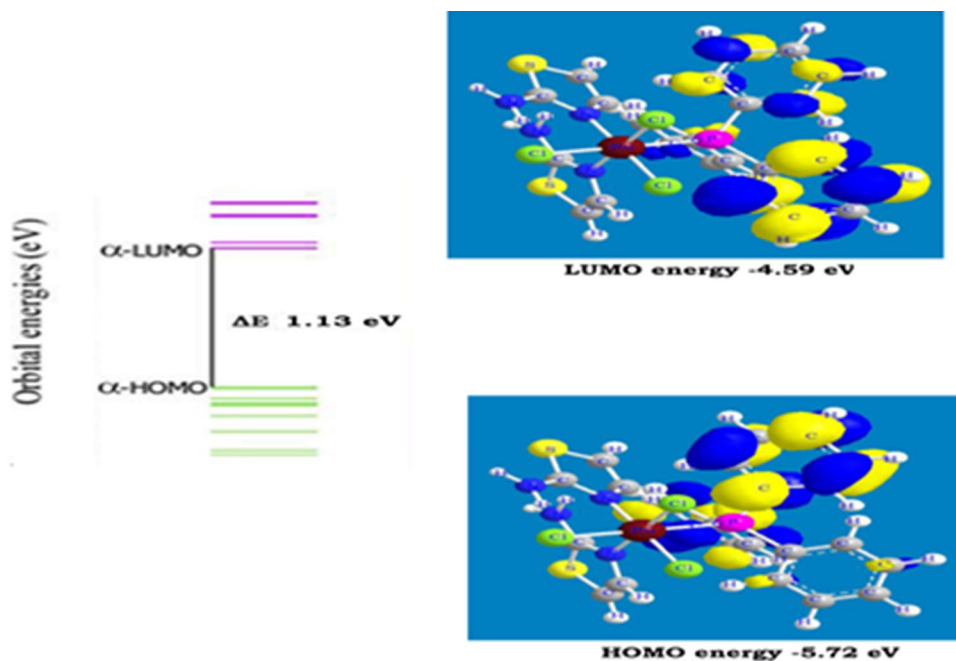


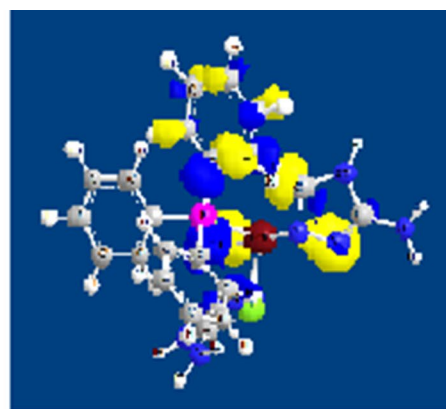
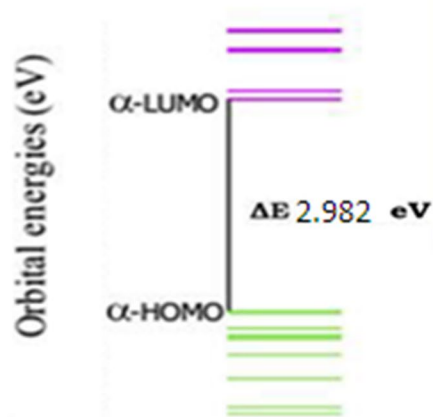
**Fig. 17** HOMO–LUMO of  $[\text{RuCl}_3(\text{Pph}_3)(\text{Ath})_2]$



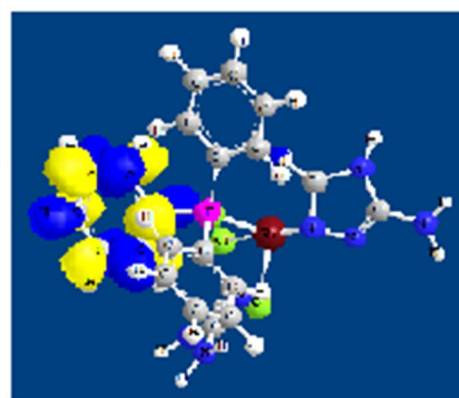
for visualisation of optimised structures. The selected bond length, bond angle and dihedral angle is represented. The HOMO–LUMO energy band gap of the above complexes respectively found.

The optimised geometry determined by DFT studies, the bond lengths and bond angles as well as HOMO and LUMO energy of all the complexes determined. In  $[\text{RuCl}_2(\text{Pph}_3)(\text{Ath})_2]$  and  $[\text{RuCl}_2(\text{Pph}_3)(\text{Atz})_2]$  the bond

length, bond angles and the energy difference between HOMO and LUMO are represented in Figs. 13, 14, 15, 16, 17, 18. The minimum energy for HOMO of  $[\text{RuCl}_3(\text{Pph}_3)(\text{Ath})_2]$  is  $-5.72$  eV while, that for LUMO is  $-4.59$  eV. The HOMO–LUMO energy band gap of the complexes is important for the electron transfer within the molecule. The HOMO–LUMO energy band gap of  $[\text{RuCl}_3(\text{Pph}_3)(\text{Ath})_2]$  is found to be  $1.13$  eV. In  $[\text{RuCl}_3(\text{Pph}_3)(\text{Atz})_2]$  complex,

**Fig. 18** HOMO–LUMO of  $\text{RuCl}_3(\text{Pph}_3)(\text{Atz})_2$ 

LUMO energy - 11.059 eV



HOMO energy -14.071 eV

**Table 3** Selected structural parameters of  $[\text{RuCl}_3(\text{Pph}_3)(\text{Ath})_2]$ 

Bond	Bond length (Å)	Angle	(°)	Dihedral angle	(°)
C(24)–H(43)	1.122	C(26)–N(31)–H(37)	119.999	H(42)–C(29)–N(30)–N(28)	164.211
P(25)–Ru(32)	2.344	H(36)–N(31)–H(37)	119.999	H(42)–C(29)–N(30)–Ru(32)	47.259
C(26)–N(27)	1.429	N(5)–Ru(32)–P(25)	90.000	N(28)–N(30)–Ru(32)–N(5)	60.000
C(26)–N(28)	1.244	N(5)–Ru(32)–N(30)	90.000	N(28)–N(30)–Ru(32)–P(25)	– 30.000
C(26)–N(31)	1.446	N(5)–Ru(32)–Cl(33)	90.000	N(28)–N(30)–Ru(32)–Cl(33)	– 30.000
N(27)–C(29)	1.446	N(5)–Ru(32)–Cl(34)	90.000	N(28)–N(30)–Ru(32)–Cl(34)	179.597
N(27)–H(40)	1.028	N(5)–Ru(32)–Cl(35)	180.000	N(28)–N(30)–Ru(32)–Cl(35)	– 120.000
N(28)–N(30)	1.352	P(25)–Ru(32)–N(30)	90.000	C(29)–N(30)–Ru(32)–N(5)	173.432
C(29)–N(30)	1.446	P(25)–Ru(32)–Cl(33)	0.573	C(29)–N(30)–Ru(32)–P(25)	83.432
C(29)–H(42)	1.122	P(25)–Ru(32)–Cl(34)	90.000	C(29)–N(30)–Ru(32)–Cl(33)	83.432
N(30)–Ru(32)	1.926	P(25)–Ru(32)–Cl(35)	90.000	C(29)–N(30)–Ru(32)–Cl(34)	– 66.971
N(31)–H(36)	1.028	N(30)–Ru(32)–Cl(33)	89.427	C(29)–N(30)–Ru(32)–Cl(35)	– 6.568
N(31)–H(37)	1.028	N(30)–Ru(32)–Cl(34)	0.000		
Ru(32)–Cl(33)	2.240	N(30)–Ru(32)–Cl(35)	90.000		
Ru(32)–Cl(34)	2.240	Cl(33)–Ru(32)–Cl(34)	89.427		
Ru(32)–Cl(35)	2.240	Cl(33)–Ru(32)–Cl(35)	90.000		
		Cl(34)–Ru(32)–Cl(35)	90.000		

**Table 4** Selected structural parameters of [RuCl<sub>3</sub>(Pph<sub>3</sub>)(Atz)<sub>2</sub>]

Bond	Bond length (Å)	Angle (°)	Dihedral angle (°)
C(35)–H(66)	1.122	N(9)–Ru(59)–N(16)	72.177
N(36)–C(37)	1.105	N(9)–Ru(59)–N(38)	65.585
N(36)–H(63)	1.028	N(9)–Ru(59)–N(45)	144.109
C(37)–N(38)	1.125	N(9)–Ru(59)–Cl(60)	138.670
C(37)–C(39)	1.155	N(9)–Ru(59)–Cl(61)	41.330
N(38)–N(59)	1.741	N(16)–Ru(59)–N(38)	137.586
C(39)–C(40)	1.118	N(16)–Ru(59)–N(45)	143.604

**Table 5** Selected structural parameters of [LaCl<sub>3</sub>(Pph<sub>3</sub>)(Ath)<sub>2</sub>]

Bond	Bond length (Å)	Angle (°)	Dihedral angle (°)
N(1)–C(2)	1.446	N(1)–C(2)	1.446
N(1)–C(3)	1.446	N(1)–C(3)	1.446
N(1)–La(32)	2.366	N(1)–La(32)	2.366
C(2)–S(4)	1.790	C(2)–S(4)	1.790
C(2)–N(6)	1.446	C(2)–N(6)	1.446
C(3)–C(5)	1.324	C(3)–C(5)	1.324
C(3)–H(53)	1.122	C(3)–H(53)	1.122
S(4)–C(5)	1.743	S(4)–C(5)	1.743
C(5)–H(41)	1.122	C(5)–H(41)	1.122
N(6)–H(38)	1.028	N(6)–H(38)	1.028
N(6)–H(39)	1.028	N(6)–H(39)	1.028
N(7)–C(8)	1.446	N(7)–C(8)	1.446
N(7)–C(9)	1.446	N(7)–C(9)	1.446
N(7)–La(32)	2.366	N(7)–La(32)	2.366
C(8)–S(10)	1.790	C(8)–S(10)	1.790
		C(8)–N(12)	1.446
		C(9)–C(11)	1.324

the energy observed for HOMO is – 14.071 while, for LUMO – 11.059 eV. The HOMO–LUMO energy band gap found to be 2.982 eV indicating that the aminothiazole containing ruthenium complex having easy electron excitation when compared to the ruthenium complex containing aminotriazole Figs. 17, 18.

The bond length and bond angles between Ru and donor atoms of different ligands are given in Tables 3, 4. The Ru–P of triphenyl phosphine found to be 2.344 Å and Ru–N of amino thiazole ligand has bond length 1.926 Å while Ru–Cl found to be 2.240 Å. The N–Ru–Cl bond angle is 89.427° similarly, Cl–Ru–Cl is 89.427° and another N–Ru–P angle found to have 90°. The bond lengths and bond angles indicate that the distorted octahedral geometry for the complex. Similarly, for other complexes the bond lengths and bond angles have been recorded and collected in Tables 3, 4, 5, 6, 7, 8.

In the case of [LaCl<sub>3</sub>(Pph<sub>3</sub>)(Ath)<sub>2</sub>] and [LaCl<sub>3</sub>(Pph<sub>3</sub>)(Atz)<sub>2</sub>] the energy for HOMO found to be – 8.57 and – 7.442 respectively while that for LUMO is – 8.06 and – 5.722 eV respectively, Figs. 19, 20, 21, 22, 23, 24. The HOMO–LUMO energy band gap (ΔE) for these two complexes are 0.51 and 1.722 eV respectively, indicating that the previous complex has more easier electron excitation compared to the latter one. Similarly, for [CeCl<sub>3</sub>(Pph<sub>3</sub>)(Ath)<sub>2</sub>] and [CeCl<sub>3</sub>(Pph<sub>3</sub>)(Atz)<sub>2</sub>] complexes Figs. 25, 26, 27, 28, 29, 30, the energy for HOMO obtained is to be – 7.941 and 5.703 respectively while, that for LUMO is – 4.444 and – 3.154 eV respectively. The HOMO–LUMO energy band gap (ΔE) in the case of [CeCl<sub>3</sub>(Pph<sub>3</sub>)(Ath)<sub>2</sub>] is 3.497 eV while, in the case of [CeCl<sub>3</sub>(Pph<sub>3</sub>)(Atz)<sub>2</sub>], it is found to be less by amount 2.549 eV, this is a clear indication that the complex containing aminotriazole has lower excitation energy.

**Table 6** Selected structural parameters of [LaCl<sub>3</sub>(Pph<sub>3</sub>)(Atz)<sub>2</sub>]

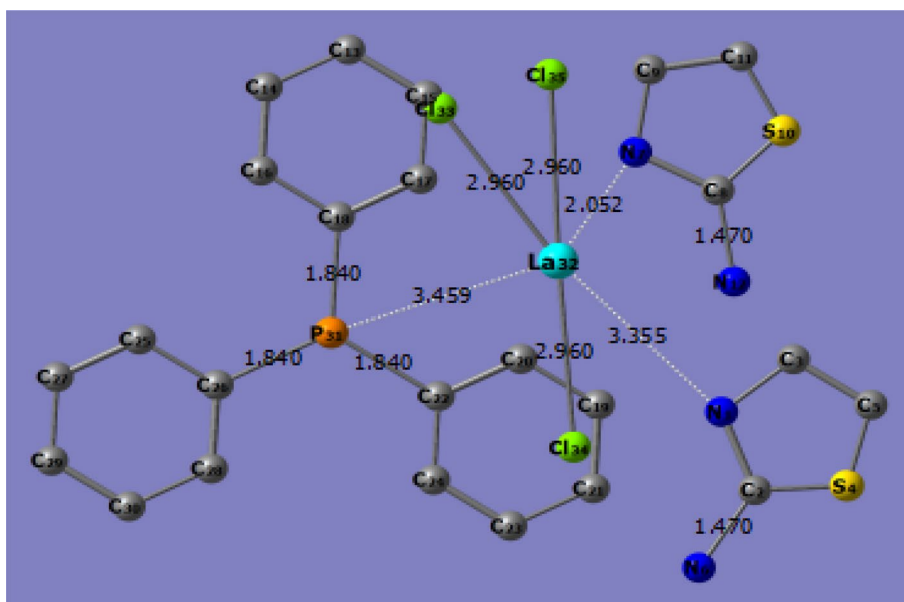
Bond	Bond length (Å)	Angle (°)	Dihedral angle (°)
C(13)–C(15)	1.386	C(26)–N(31)–H(37)	119.999
C(13)–P(19)	1.864	H(36)–N(31)–H(37)	119.999
C(14)–C(16)	1.386	P(19)–La(32)–N(24)	90.000
C(14)–H(48)	1.122	P(19)–La(32)–N(30)	90.000
C(15)–C(17)	1.386	P(19)–La(32)–Cl(33)	90.000
C(15)–H(47)	1.122	P(19)–La(32)–Cl(34)	90.000
C(16)–C(18)	1.386	P(19)–La(32)–Cl(35)	180.000
C(16)–H(46)	1.122	N(24)–La(32)–N(30)	120.000
C(17)–C(18)	1.386	N(24)–La(32)–Cl(33)	120.000
C(17)–H(45)	1.122	N(24)–La(32)–Cl(34)	150.000
C(18)–H(44)	1.122	N(24)–La(32)–Cl(35)	90.000
P(19)–La(32)	2.784	N(30)–La(32)–Cl(33)	0.000
C(20)–N(21)	1.429	N(30)–La(32)–Cl(34)	90.000
C(20)–N(22)	1.244	N(30)–La(32)–Cl(35)	90.000
C(20)–N(25)	1.446	Cl(33)–La(32)–Cl(34)	90.000
N(21)–C(23)	1.446	Cl(33)–La(32)–Cl(35)	90.000
N(21)–H(41)	1.028	Cl(34)–La(32)–Cl(35)	90.000
N(22)–N(24)	1.352	C(26)–N(31)–H(37)	119.999
C(23)–N(24)	1.446	H(36)–N(31)–H(37)	119.999
C(23)–H(43)	1.122	P(19)–La(32)–N(24)	90.000
N(24)–La(32)	2.366	P(19)–La(32)–N(30)	90.000
N(25)–H(38)	1.028	P(19)–La(32)–Cl(33)	90.000

**Table 7** Selected structural parameters of [CeCl<sub>3</sub>(Pph<sub>3</sub>)(Ath)<sub>2</sub>]

Bond	Bond length (Å)	Angle (°)	Dihedral angle (°)
N(1)–C(2)	1.446	C(2)–N(1)–C(3)	P(31)–Ce(32)
N(1)–C(3)	1.446	C(2)–N(1)–Ce(32)	124.499
N(1)–Ce(32)	2.326	C(3)–N(1)–Ce(32)	124.500
C(2)–S(4)	1.790	N(1)–C(2)–S(4)	Ce(32)–Cl(34)
C(2)–N(6)	1.446	N(1)–C(2)–N(6)	Ce(32)–Cl(35)
C(3)–C(5)	1.324	S(4)–C(2)–N(6)	C(2)–N(1)–C(3)
C(3)–H(53)	1.122	N(1)–C(3)–C(5)	C(2)–N(1)–Ce(32)
S(4)–C(5)	1.743	N(1)–C(3)–H(53)	124.498
C(5)–H(41)	1.122	C(5)–C(3)–H(53)	124.498
N(6)–H(38)	1.028	C(2)–S(4)–C(5)	N(1)–C(2)–N(6)
N(6)–H(39)	1.028	C(3)–C(5)–S(4)	S(4)–C(2)–N(6)
N(7)–C(8)	1.446	C(3)–C(5)–H(41)	N(1)–C(3)–C(5)
N(7)–C(9)	1.446	S(4)–C(5)–H(41)	125.039
N(7)–Ce(32)	2.326	C(2)–N(6)–H(38)	117.368
C(8)–S(10)	1.790		120.000

**Table 8** Selected structural parameters of  $[\text{CeCl}_3(\text{Pph}_3)(\text{Atz})_2]$ 

Bond	Bond length (Å)	Angle	(°)	Dihedral angle	(°)
C(1)–C(2)	1.386	P(19)–Ce(32)–Cl(34)	90.000	C(26)–N(28)–N(30)–Ce(32)	141.906
C(26)–N(28)	1.244	P(19)–Ce(32)–Cl(35)	180.000	N(27)–C(29)–N(30)–N(28)	–15.140
C(26)–N(31)	1.446	N(24)–Ce(32)–N(30)	120.000	N(27)–C(29)–N(30)–Ce(32)	–132.092
N(27)–C(29)	1.446	N(24)–Ce(32)–Cl(33)	120.000	H(42)–C(29)–N(30)–N(28)	164.211
N(27)–H(40)	1.028	N(24)–Ce(32)–Cl(34)	150.000	H(42)–C(29)–N(30)–Ce(32)	47.259
N(28)–N(30)	1.352	N(24)–Ce(32)–Cl(35)	90.000	N(28)–N(30)–Ce(32)–P(19)	180.000
C(29)–N(30)	1.446	N(30)–Ce(32)–Cl(33)	0.000	N(28)–N(30)–Ce(32)–N(24)	90.000
C(29)–H(42)	1.122	N(30)–Ce(32)–Cl(34)	90.000	N(28)–N(30)–Ce(32)–Cl(33)	–154.365
N(30)–Ce(32)	2.326	N(30)–Ce(32)–Cl(35)	90.000	N(28)–N(30)–Ce(32)–Cl(34)	–89.000
N(31)–H(36)	1.028	Cl(33)–Ce(32)–Cl(34)	90.000	N(28)–N(30)–Ce(32)–Cl(35)	0.000
N(31)–H(37)	1.028	Cl(33)–Ce(32)–Cl(35)	90.000	C(29)–N(30)–Ce(32)–P(19)	–66.568
Ce(32)–Cl(33)	2.640			C(29)–N(30)–Ce(32)–N(24)	–156.568
Ce(32)–Cl(34)	2.640			C(29)–N(30)–Ce(32)–Cl(33)	–40.933
Ce(32)–Cl(35)	2.640			C(29)–N(30)–Ce(32)–Cl(34)	23.432

**Fig. 19** Optimized geometry & Standard bond length of  $[\text{LaCl}_3(\text{Pph}_3)(\text{Ath})_2]$ 

## 6 Biological Activities

### 6.1 DNA Binding Experiments

The binding interaction of only two complexes with *CT*-DNA was monitored by comparing their absorption spectra with and without *CT*-DNA. The Figs. 31, 32 represents the absorption spectra of the  $[\text{RuCl}_3(\text{Pph}_3)(\text{Ath})_2]$  and  $[\text{RuCl}_3(\text{Pph}_3)(\text{Atz})_2]$  respectively, in the presence and absence of *CT*-DNA and both the complexes exhibited well resolved bands at 270–280 nm with increasing the DNA concentration (0–50  $\mu\text{M}$ ). The  $K_b$  values obtained for  $[\text{RuCl}_3(\text{Pph}_3)(\text{Ath})_2]$  and  $[\text{RuCl}_3(\text{Pph}_3)(\text{Atz})_2]$  are 4.02 and  $4.55 \times 10^5 \text{ M}^{-1}$  respectively in the region 270–280 nm with increasing concentration of DNA. The

intrinsic binding constant value suggests that the interactions of complexes with *CT*-DNA as tabulated in Table 9. It is clear that, the intense absorption bands observed for the free metal complexes is in the region 295–320 nm, while for bound, it is in the range 297–322 nm, suggests  $\pi \rightarrow \pi^*$  transitions. As the concentration of the *CT* DNA increases, a slight red shift and hypochromism of about 2–3 nm range was exhibited by the metal complexes. Red shift and hypochromicity is the feature observed when intercalative binding mode is present due to the strong stacking interactions between the base pairs of DNA and the aromatic chromospheres of the complexes. Also, the intrinsic binding constant values were evaluated by the change in the absorbance values as the DNA concentration increases gradually [31, 32].

**Fig. 20** Optimized geometry & Standard bond length of  $[\text{LaCl}_3(\text{Pph}_3)(\text{Atz})_2]$

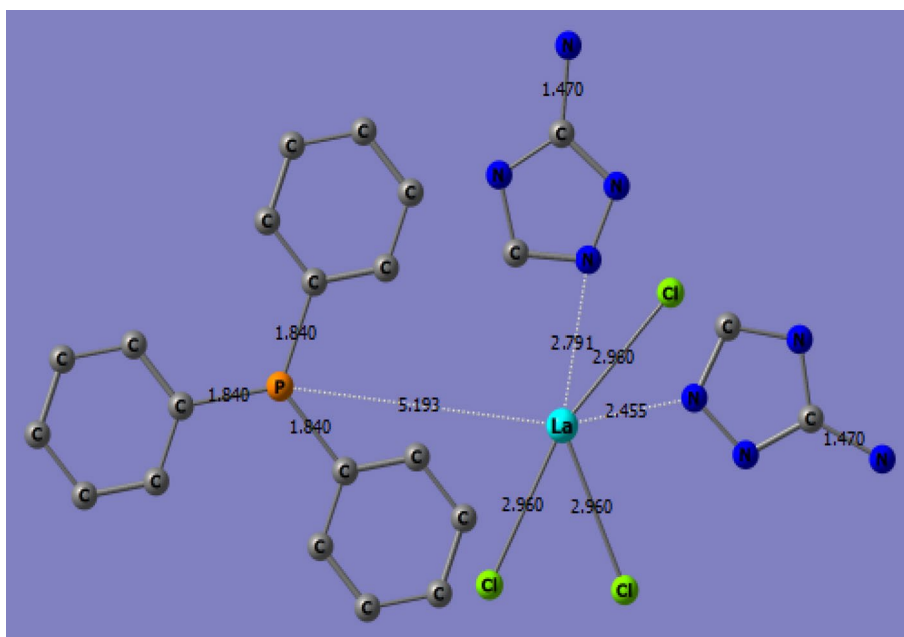
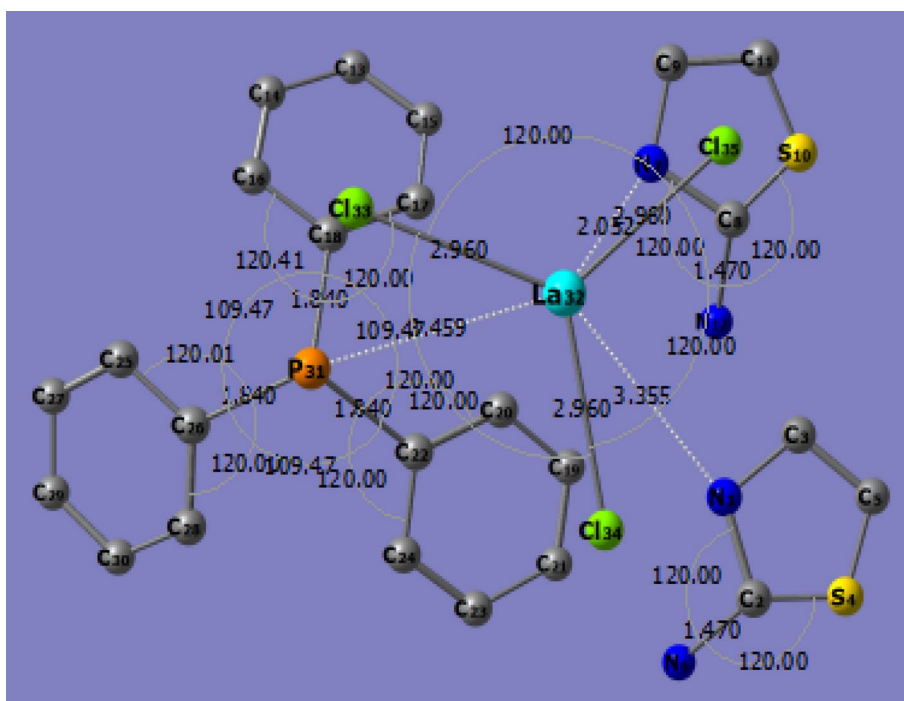


**Fig. 21** Standard bond angle of  $[\text{LaCl}_3(\text{Pph}_3)(\text{Ath}_2)]$



## 6.2 Fluorescence Quenching

To investigate further the interaction mode between the complex and *CT*-DNA, the fluorescence titration experiments has been performed. The complexes emits luminescence in Tris-buffer with maximum wavelengths in the range 360–410 nm shows the emission spectra of the complex in the absence and presence of varying amounts of *CT*-DNA. In the emission spectra for the complex, with

increasing *CT*-DNA concentration the emission intensity is decreased due to self-stacking of some free bases in the compound along the DNA surface [59]. The experimental result provides a direct evidence for the interaction between the complexes containing aminothiazole ligand with Ru(III), Ce(III), La(III) and *CT* DNA through the groove binding mode are shown in Figs. 33, 34, 35, 36. The fluorescence quenching of DNA with increasing concentration of metal complexes were expressed in terms of  $K_{sv}$  values calculated



**Fig. 22** Standard bond angle of  $[\text{LaCl}_3(\text{Pph}_3)(\text{Atz})_2]$

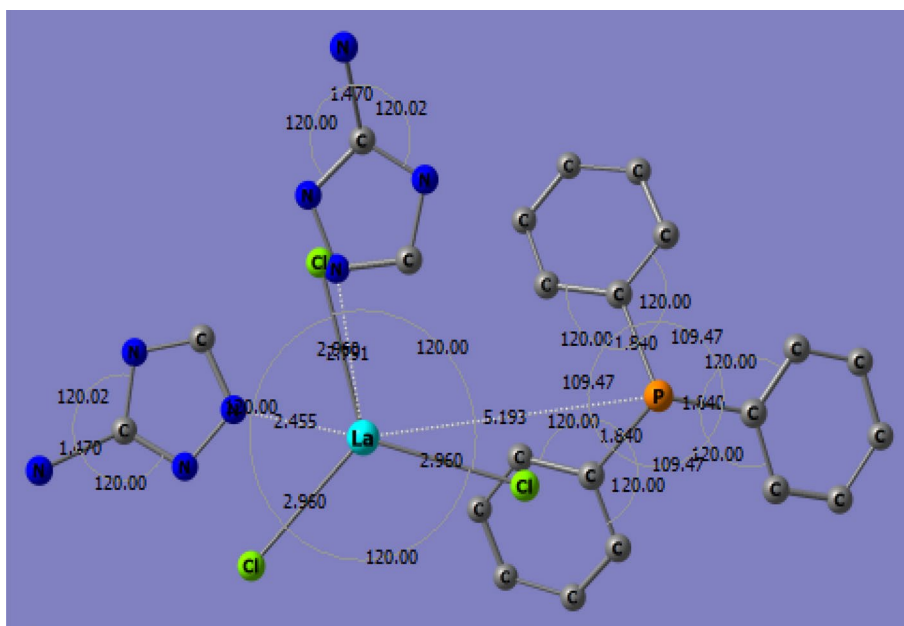


**Fig. 23** HOMO–LUMO of  $[\text{LaCl}_3(\text{Pph}_3)(\text{Ath})_2]$

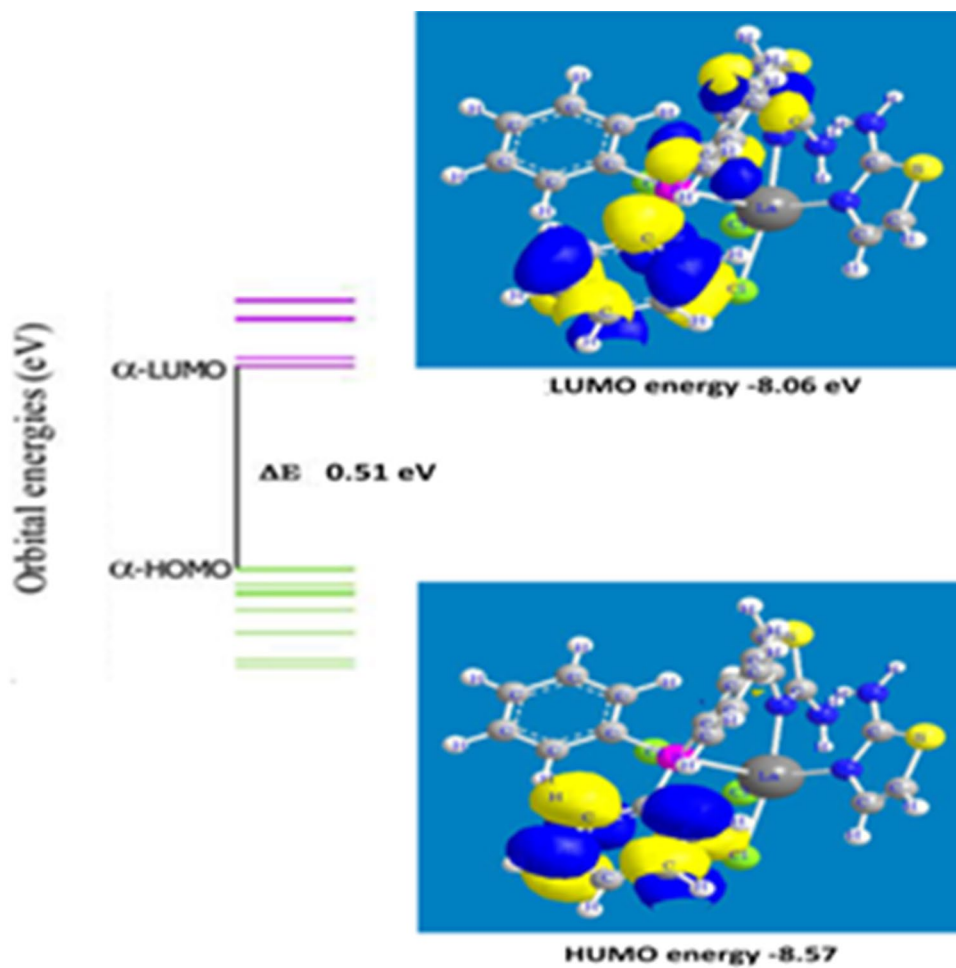


**Fig. 24** HOMO–LUMO of  
[LaCl<sub>3</sub>(PPh<sub>3</sub>)(Atz)<sub>2</sub>]

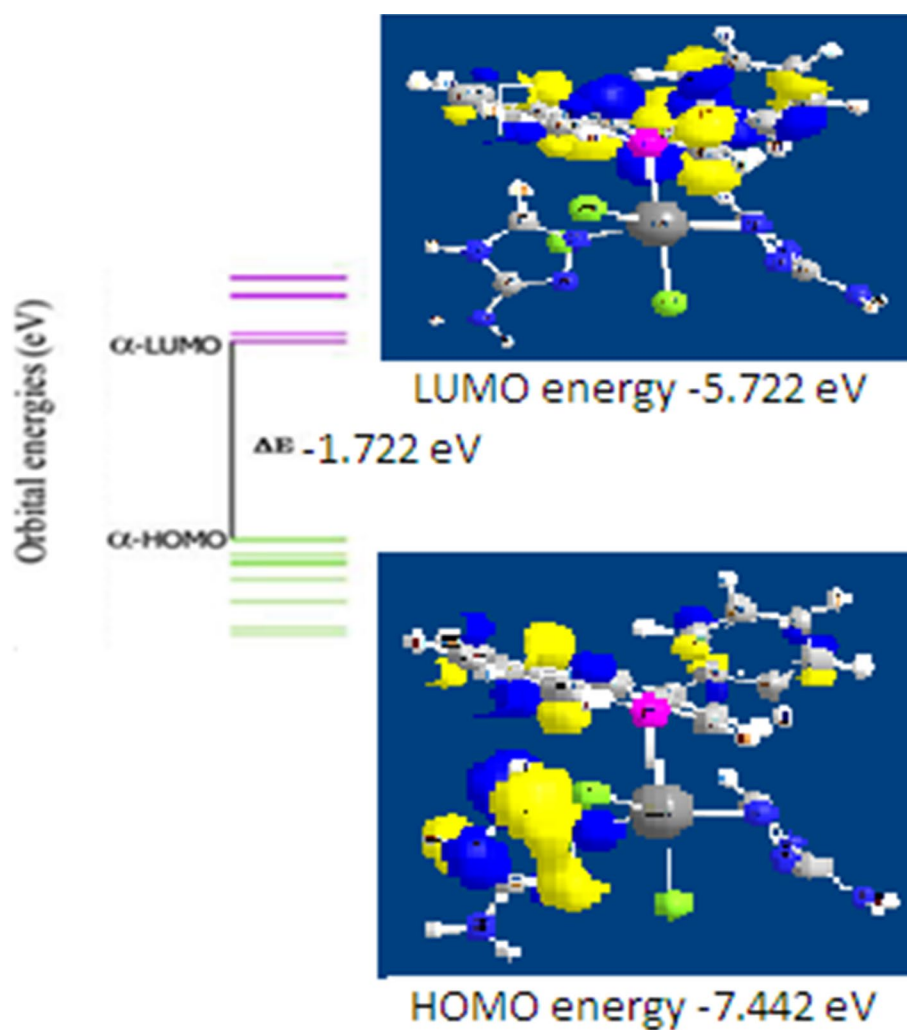


**Fig. 25** Optimised geometry and standard bond length of  
[CeCl<sub>3</sub>(PPh<sub>3</sub>)(Ath)<sub>2</sub>]

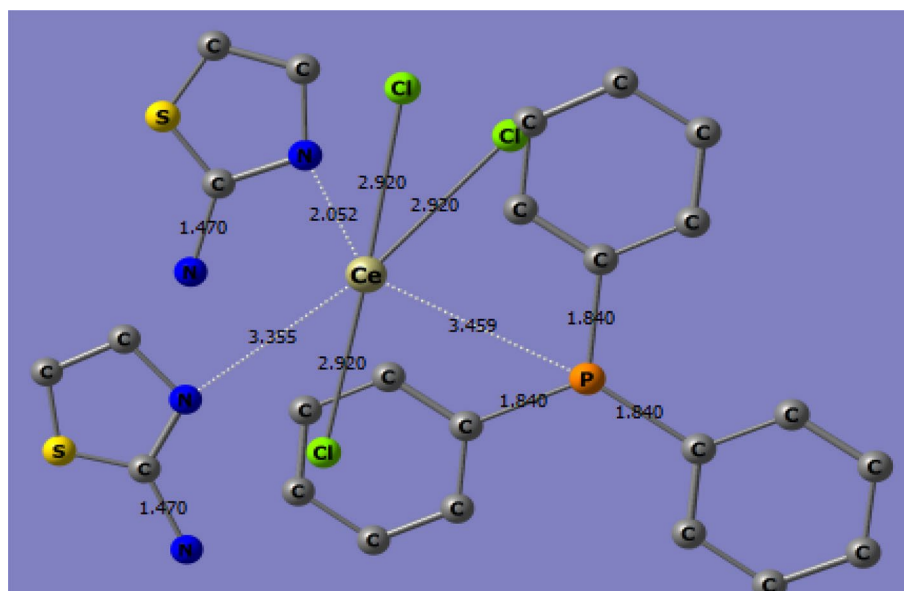


**Fig. 26** Optimised geometry and standard bond length of  $[\text{CeCl}_3(\text{Pph}_3)(\text{Atz})_2]$

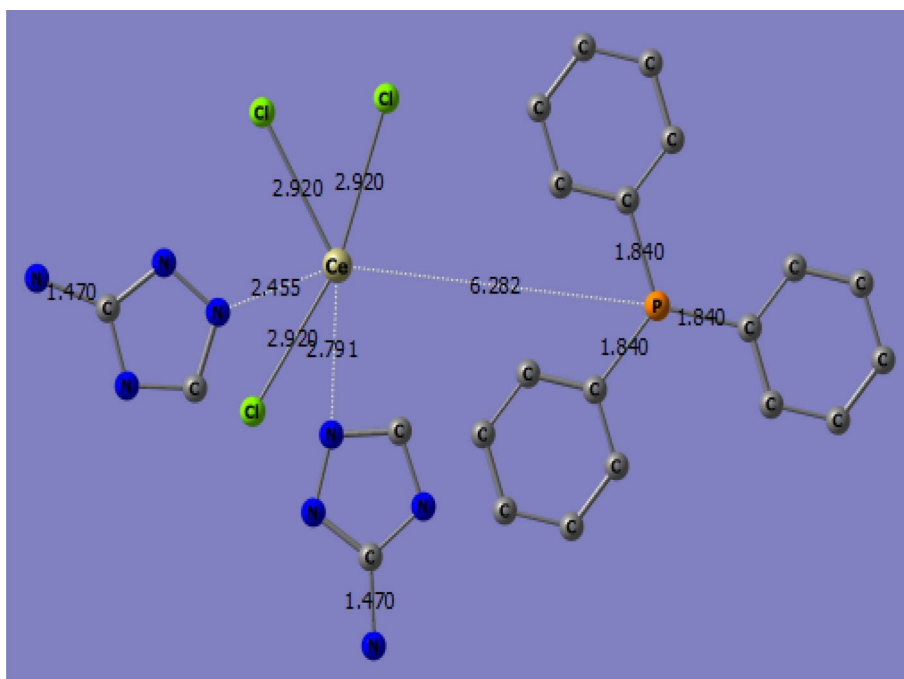
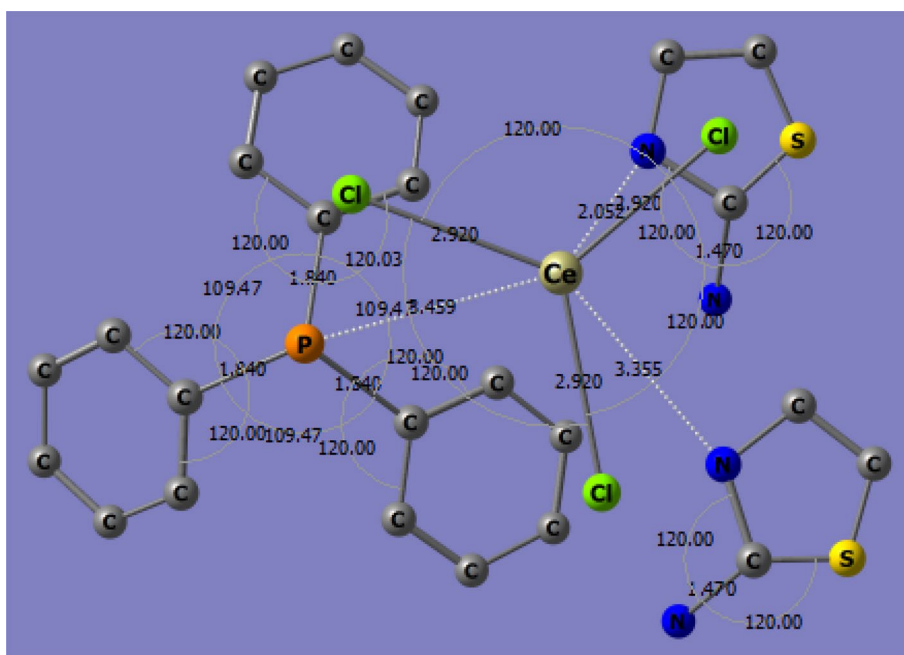


**Fig. 27** Standard bond angles of  $[\text{CeCl}_3(\text{Pph}_3)(\text{Ath})_2]$



from slope of plot  $I_0/I$  versus  $r$ . The binding constant  $K_{sv}$  values are found to be  $5.683 \times 10^4 \text{ M}^{-1}$ ,  $5.241 \times 10^4 \text{ M}^{-1}$  and  $6.203 \times 10^4 \text{ M}^{-1}$  respectively for Ru(II), Ce(II) and La(II) complexes which are consistent with the values observed in other groove binding systems [33]. The quenching may be due to the complexes interacting with DNA through an groove mode and it is clear from  $K_{sv}$  values. All the complexes bound strongly with DNA, which is confirmed with the electronic absorption study.

### 6.3 Antimicrobial Activity

The different microorganisms such as, two Gram-positive (*S. aureus*, *B. subtilis*) as well as two Gram-negative (*E. coli*, *S. typhi*) bacteria and two yeasts (*A. niger*, *C. albicans*) were used to study the biological activity of ligands and all the four complexes. In general, all the complexes showed higher activity for Gram (+) than for Gram (−) bacteria, but slightly higher activity observed in complexes containing triazole ligand

**Fig. 28** Standard bond angles of  $[\text{CeCl}_3(\text{Pph}_3)(\text{Atz})_2]$

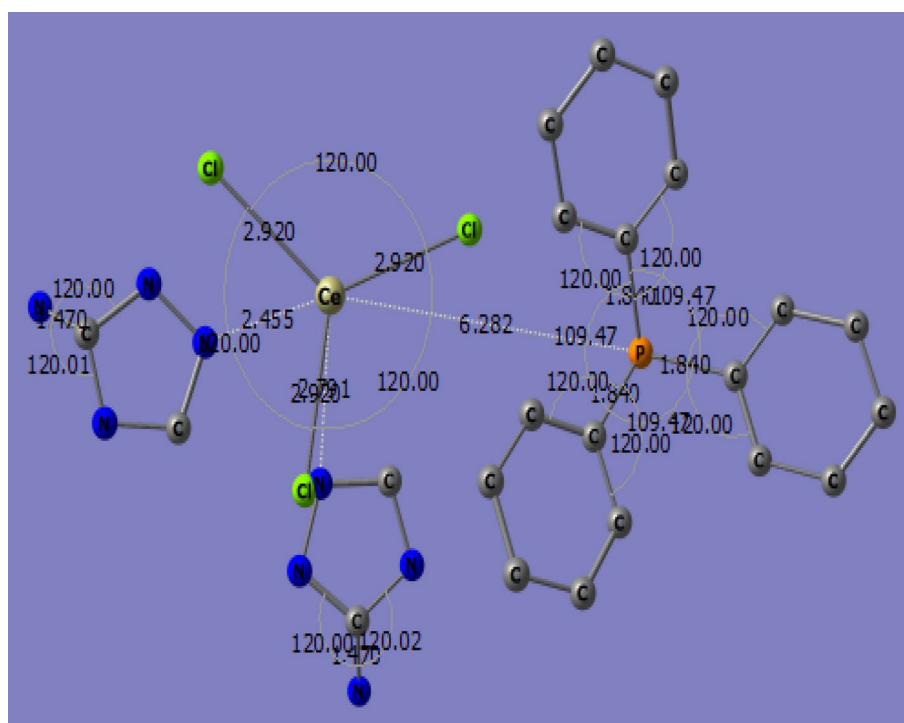


**Fig. 29** HOMO–LUMO of  $[\text{CeCl}_3(\text{Pph}_3)(\text{Atz})_2]$

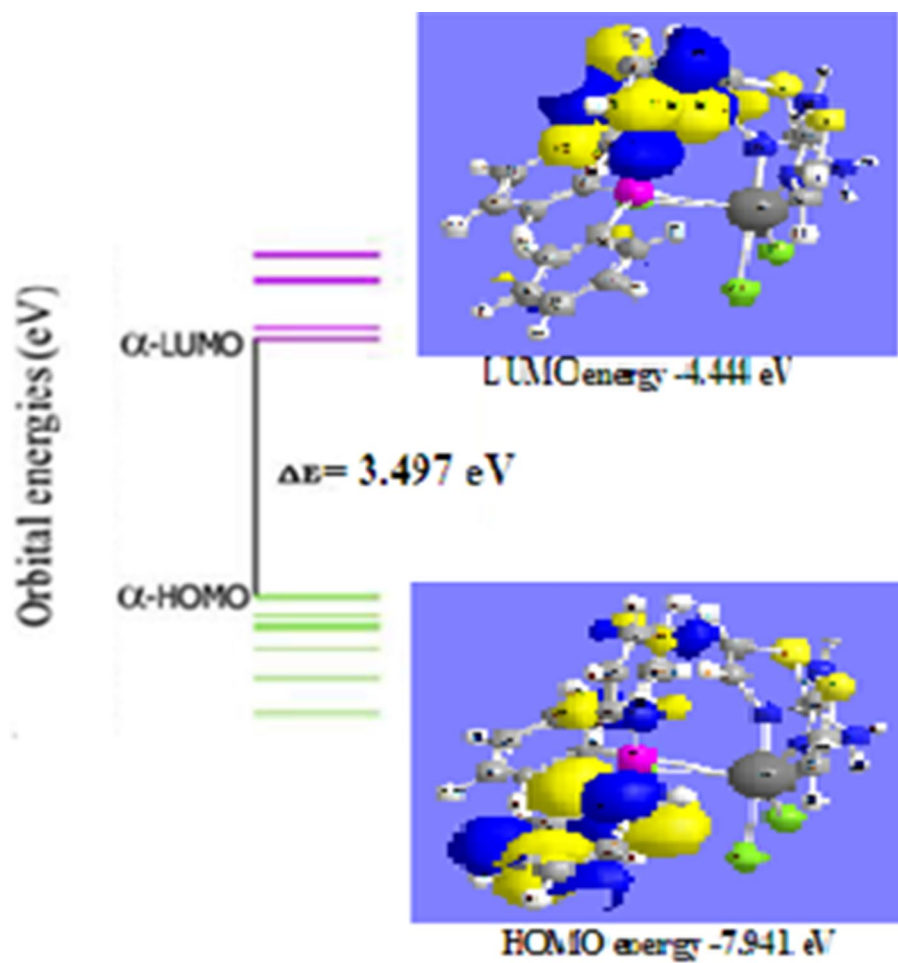


**Fig. 30** HOMO–LUMO of  $[\text{CeCl}_3(\text{Pph}_3)(\text{Atz})_2]$

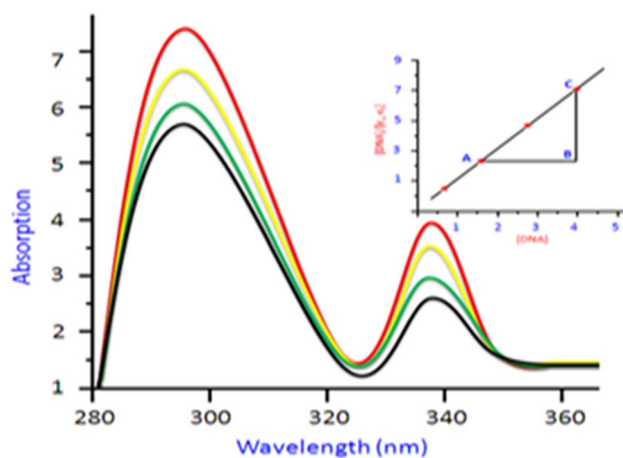
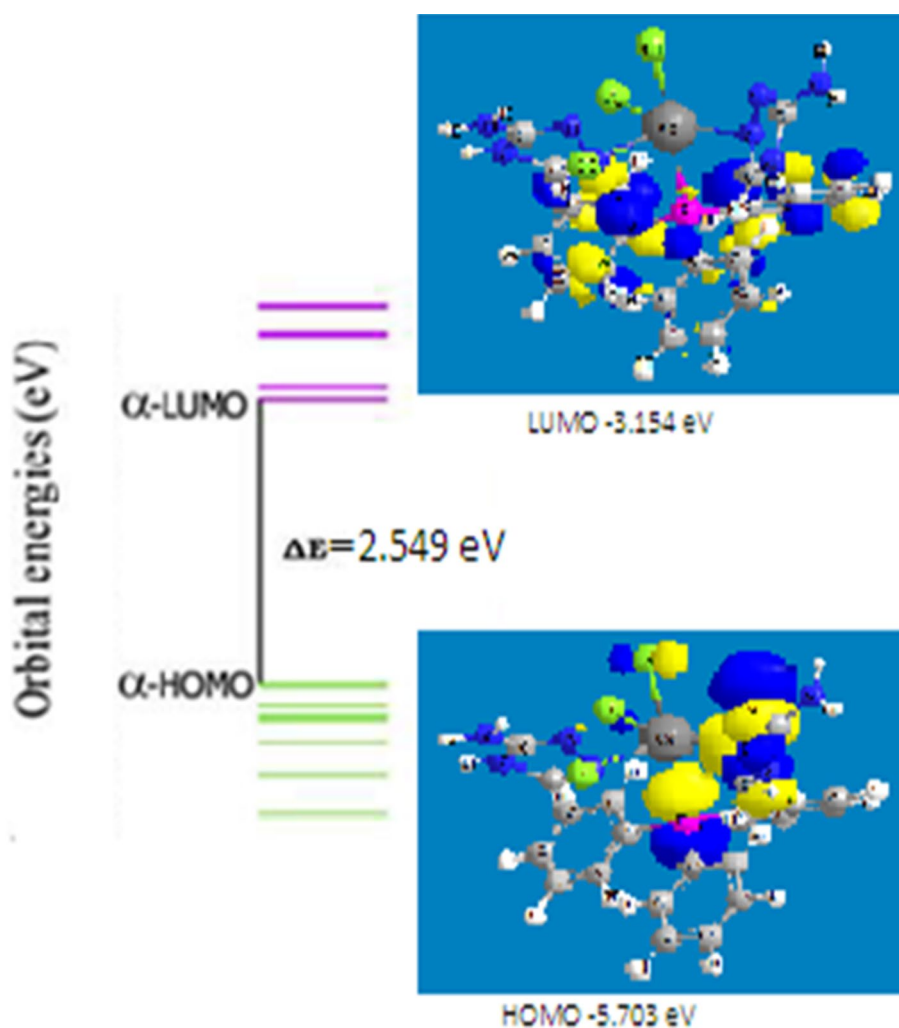


**Fig. 31** Electronic absorption spectra of the  $[\text{RuCl}_3(\text{Pph}_3)(\text{Ath})_2]$  complex in buffer solution (5 mM Tris–HCl/10 mM NaCl at pH 7.2). Plot  $[\text{Ru}] = 10 \mu\text{M}$ ,  $[\text{DNA}] = 0\text{--}50 \mu\text{M}$

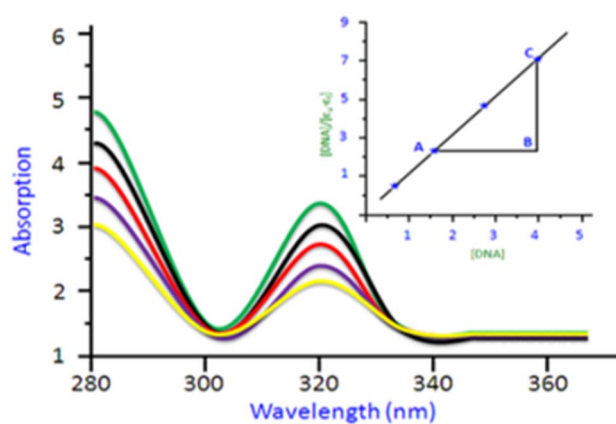


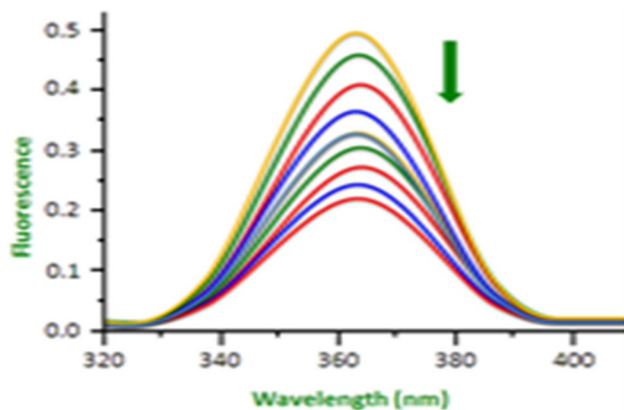
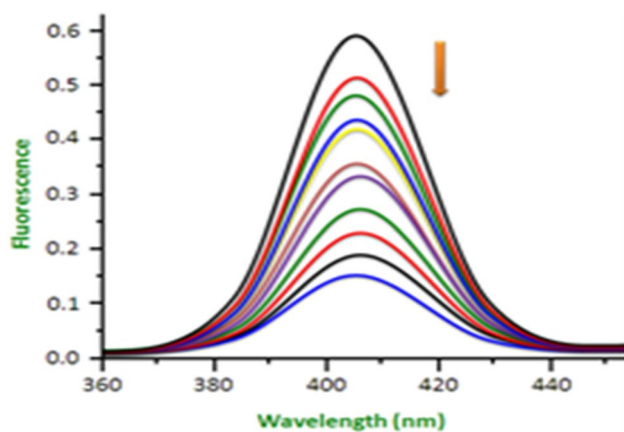
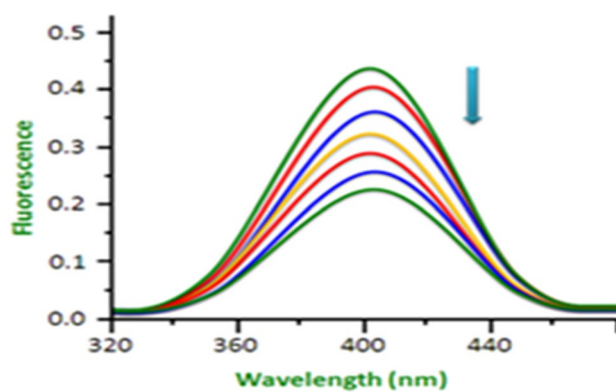
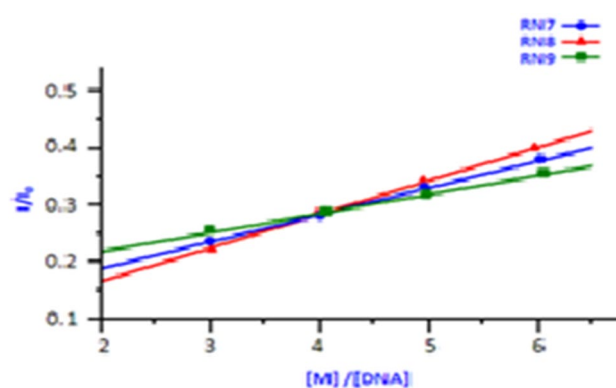
**Fig. 32** Absorption spectra of in  $[\text{RuCl}_3(\text{Pph}_3)(\text{Atz})_2]$  Tris–HCl buffer upon addition of DNA.  $[\text{Ru}] = 10 \mu\text{M}$ ,  $[\text{DNA}] = 0\text{--}50 \mu\text{M}$

(Table 10). The highest active compound for Gram (–) bacteria was complex  $[\text{RuCl}_3(\text{Pph}_3)(\text{Atz})_2]$  while the complexes  $[\text{RuCl}_3(\text{Pph}_3)(\text{Atz})_2]$  and  $[\text{CeCl}_3(\text{Pph}_3)(\text{Atz})_2]$  showed highest

activity for Gram (+) bacteria. The results revealed that both complexes are excellent antifungal agents. The higher activity of the metal complexes is may be due to the smaller sized metal ions which enhance the polar nature of the complex to

**Table 9** Electronic absorption data upon addition of CT-DNA to the complexes

Complex	$\lambda_{\max}$ (nm)		$\Delta\lambda$ (nm)	H (%)	Binding constant $K_b$ ( $M^{-1}$ )
	Free	Bound			
[RuCl <sub>3</sub> (PPh <sub>3</sub> )(Atz)]	295	298	2	8.34	$4.02 \times 10^5$
[RuCl <sub>3</sub> (PPh <sub>3</sub> )(Atz)]	320	322	2	9.15	$4.55 \times 10^5$

**Fig. 33** Emission spectra of the [RuCl<sub>3</sub>(PPh<sub>3</sub>)(Ath)<sub>2</sub>] complex at room temperature in Tris–HCl/NaCl buffer solution (pH 7.2) in the absence and presence of FS-DNA,  $\lambda_{\text{ex}} = 363$  nm. The arrow shows the intensity changes upon increasing the concentration of FS-DNA (0.0–38.1  $\mu\text{M}$ )**Fig. 34** Emission spectra of the [LaCl<sub>3</sub>(PPh<sub>3</sub>)(Ath)<sub>2</sub>] complex at room temperature in Tris–HCl/NaCl buffer solution (pH = 7.2) in the absence and presence of FS-DNA,  $\lambda_{\text{ex}} = 410$  nm. The arrow shows the intensity changes upon increasing the concentration of FS-DNA (0.0–38.1  $\mu\text{M}$ )**Fig. 35** Emission spectra of the [CeCl<sub>3</sub>(PPh<sub>3</sub>)(Ath)<sub>2</sub>] complex at room temperature in Tris–HCl/NaCl buffer solution (pH 7.2) in the absence and presence of FS-DNA,  $\lambda_{\text{ex}} = 404$  nm. The arrow shows the intensity changes upon increasing the concentration of FS-DNA (0.0–38.1  $\mu\text{M}$ )**Fig. 36** Plot of  $I_0/I$  vs. [DNA] for [RuCl<sub>3</sub>(PPh<sub>3</sub>)(Ath)<sub>2</sub>], [LaCl<sub>3</sub>(PPh<sub>3</sub>)(Ath)<sub>2</sub>] and [CeCl<sub>3</sub>(PPh<sub>3</sub>)(Ath)<sub>2</sub>]

larger extent which leads to the increase in lipophilicity. These results are in good correlation with the DNA interaction and docking studies of the metal complexes [34, 35].

#### 6.4 Antioxidant Activity Using the DPPH Method

The DPPH radical scavenging activity data represented in Table 11. DPPH solution in methanol gives strong absorbance at 517 nm. The synthesized metal complexes were screened for antioxidant activity against DPPH radical at 10–100  $\mu\text{g}/\text{mL}$  concentration. The antioxidant activities of the synthesized compounds are expressed by comparing with standard BHT. All the complexes exhibited good antioxidant activity compared to the standard [36, 37]. The equation below has been used to obtain the percentage of scavenged DPPH radical:

$$\text{Percentage scavenging activity} = \frac{\text{Absorbance of control} - \text{Absorbance of sample}}{\text{Absorbance of control}} \times 100$$

**Table 10** In-vitro antimicrobial activity of compounds and their inhibition zone (MIC) in mm

Compd\Conc. ( $\mu\text{g/mL}$ )	Antibacterial activity								Antifungal activity			
	<i>E. coli</i>		<i>S. typhi</i>		<i>S. aureus</i>		<i>B. subtilis</i>		<i>A. niger</i>		<i>C. albicans</i>	
	100	200	100	200	100	200	100	200	100	200	100	200
[RuCl <sub>3</sub> (Pph <sub>3</sub> )(Ath) <sub>2</sub> ]	19	20	17	19	22	21	22	26	19	25	17	20
[RuCl <sub>3</sub> (Pph <sub>3</sub> )(Atz) <sub>2</sub> ]	18	24	16	21	22	23	20	29	19	25	18	20
[LaCl <sub>3</sub> (Pph <sub>3</sub> )(Ath) <sub>2</sub> ]	19	25	17	20	21	22	22	29	20	24	17	19
[LaCl <sub>3</sub> (Pph <sub>3</sub> )(Atz) <sub>2</sub> ]	18	24	19	20	19	24	23	31	17	21	20	21
[CeCl <sub>3</sub> (Pph <sub>3</sub> )(Ath) <sub>2</sub> ]	15	13	17	21	19	22	24	30	18	22	21	22
[CeCl <sub>3</sub> (Pph <sub>3</sub> )(Atz) <sub>2</sub> ]	16	17	15	20	20	26	19	25	18	24	19	19
Std 1	25	28	24	27	25	30	28	34	–	–	–	–
Std 2	–	–	–	–	–	–	–	–	26	30	22	26
Control	–	–	–	–	–	–	–	–	–	–	–	–

Where Std1. is chloramphenicol, Std2. is fluconazole, control is DMSO

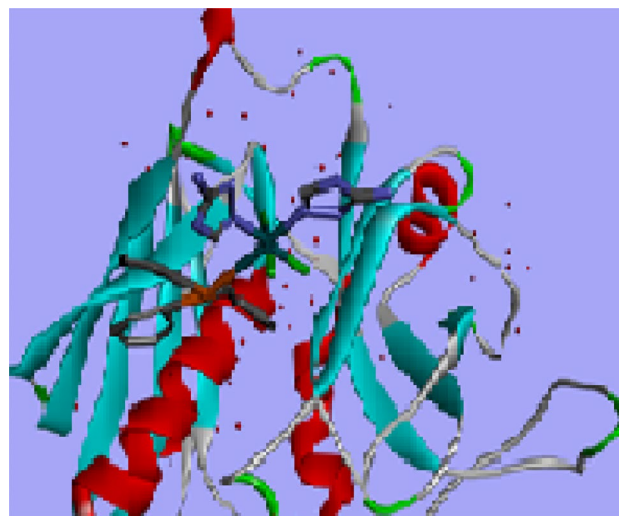
**Table 11** Antioxidant activity of the synthesized compounds

Compounds	% of Scavenging activity at different concentrations in $\mu\text{g/mL}$									
	10	20	30	40	50	60	70	80	90	100
[RuCl <sub>3</sub> (Pph <sub>3</sub> )(Ath) <sub>2</sub> ]	21.12	29.28	46.51	51.21	61.13	70.15	73.72	74.29	82.31	81.11
[RuCl <sub>2</sub> (Pph <sub>3</sub> )(Atz) <sub>2</sub> Cl]	18.12	27.17	36.94	41.19	47.22	66.17	71.25	81.12	82.13	88.23
[LaCl <sub>3</sub> (Pph <sub>3</sub> )(Ath) <sub>2</sub> ]	19.44	24.56	42.31	41.62	57.52	67.61	72.18	79.17	83.41	87.61
[LaCl <sub>3</sub> (Pph <sub>3</sub> )(Atz) <sub>2</sub> ]	20.22	30.31	35.32	40.92	45.63	58.31	58.57	66.17	68.53	71.33
[CeCl <sub>3</sub> (Pph <sub>3</sub> )(Ath) <sub>2</sub> ]	19.51	29.45	38.77	44.14	47.52	51.15	54.89	63.56	67.58	73.41
[CeCl <sub>2</sub> (Pph <sub>3</sub> )(Atz) <sub>2</sub> Cl]	21.32	28.32	36.52	40.76	44.67	49.35	58.92	68.59	69.03	71.33
BHT	32.43	38.94	50.21	56.78	65.47	78.24	85.83	92.53	94.87	97.56

**Fig. 37** Antibacterial docking of [RuCl<sub>3</sub>(pph<sub>3</sub>)(Ath)<sub>2</sub>] Docking score – 325.02 kJ/mol<sup>-1</sup>

## 6.5 Molecular Docking Studies

In order to understand and to support in-vitro biological potency of the synthesized metal complexes and DNA

**Fig. 38** Antibacterial docking of [RuCl<sub>3</sub>(Pph<sub>3</sub>)(Atz)<sub>2</sub>]: Docking score – 331.25 kJ/mol<sup>-1</sup>

interactions docking studies has been studied. The docking used to determine the orientation of inhibitors bound in the active site of receptors. As the metal complexes exhibited good DNA binding property, in the present study 2MBR selected and human estrogen receptor which are involved in

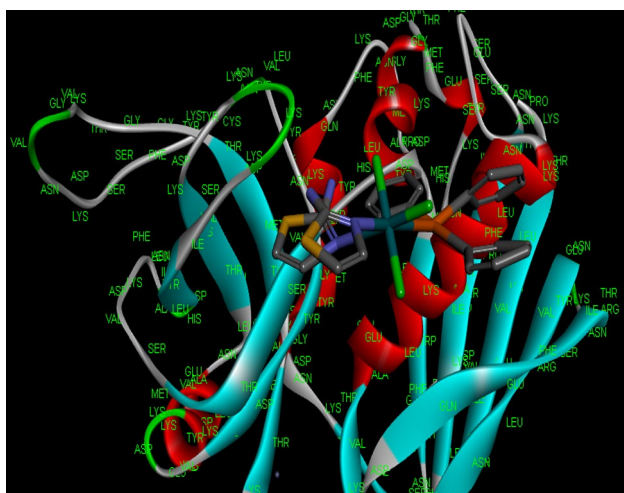


**Fig. 39**  $[\text{LaCl}_3(\text{pph}_3)(\text{Ath})_2]$  Docking score  $-321.02 \text{ kJ/mol}^{-1}$

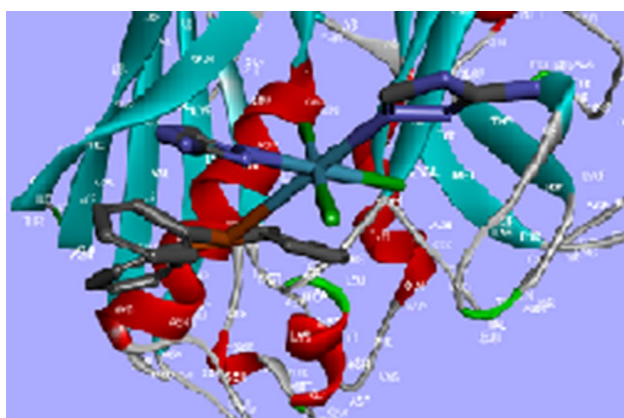


**Fig. 40**  $[\text{LaCl}_3(\text{Pph}_3)(\text{Atz})_2]$ : Docking score  $-345.19 \text{ kJ/mol}^{-1}$

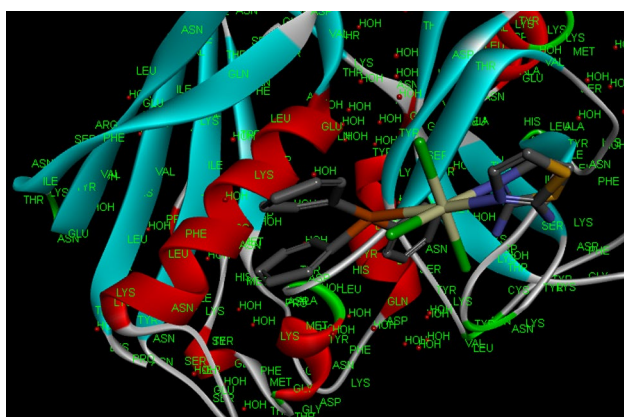


**Fig. 41**  $[\text{CeCl}_3(\text{pph}_3)(\text{Ath})_2]$ : Docking score  $-319.02 \text{ kJ/mol}^{-1}$

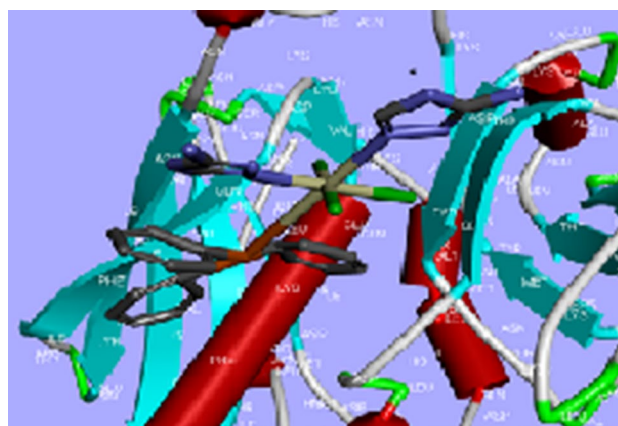


**Fig. 42**  $[\text{CeCl}_3(\text{Pph}_3)(\text{Atz})_2]$ : Docking score  $-329.52 \text{ kJ/mol}^{-1}$

cancer causing mechanism in biological system. Ciprofloxacin drug was used as standard for docking studies which was known to be potential inhibitor of human estrogen receptor.

The docking study was carried out using Hex 8.2 software; both the receptor and complex were uploaded in pdb file format. The E-Total values obtained from the HEX software after completion of docking process indicate that the strong interaction of complex with the receptors. E-Total values and their docked structure are shown in Figs. 37, 38, 39, 40, 41, 42. The complexes  $[\text{RuCl}_3(\text{Pph}_3)(\text{Ath})_2]$ ,  $[\text{LaCl}_3(\text{Pph}_3)(\text{Ath})_2]$  and  $[\text{CeCl}_3(\text{Pph}_3)(\text{Ath})_2]$  showed least docking score of  $-325.02$ ,  $-321.02$  and  $-319.02 \text{ kJ/mol}^{-1}$  respectively with the protein receptor SEC2 (PDB code: 1STE) in *Staphylococcus aureus*. On the other hand, the complexes  $[\text{RuCl}_3(\text{Pph}_3)(\text{Atz})_2]$ ,  $[\text{LaCl}_3(\text{Pph}_3)(\text{Atz})_2]$  and  $[\text{CeCl}_3(\text{Pph}_3)(\text{Atz})_2]$  exhibiting the docking score  $-331.25$ ,  $-345.19$  and  $-329.52 \text{ kJ/mol}^{-1}$  respectively. On comparing the docking results, the complexes containing aminotriazole (Atz) have slightly more negative values, indicating that they are more potential DNA binder than the complexes containing aminothiazole (Ath) ligand [38].

## 7 Conclusion

The article involves synthetic procedure of a series of triphenylphosphine complexes containing mixed ligands like; 2-aminothiazole (Ath) and 2-aminotriazole (Atz). The complexes are of the formula,  $[\text{MCl}_3((\text{Pph}_3)(\text{Ath})_2)]$  and  $[\text{MCl}_2((\text{Pph}_3)(\text{Atz})_2)]$ ,  $[\text{M} = \text{Ru(III), Ce(III) and La(III)}$ ]. A series of mixed ligand complexes were structurally characterized by different physicochemical and spectroscopic techniques. The electronic, magnetic susceptibility and molar conductance data confirmed the octahedral geometry for



the complexes. DFT studies have been carried out on all the complexes to compare the structure and properties of the complexes. Bond lengths, bond angles HOMO–LUMO, energy gap ( $\Delta E$ ) were calculated and are in a good agreement with the experimental results. Moreover, the interaction of metal complex with calf thymus DNA have been effectively examined using electronic absorption titrations and fluorescence studies, the results reveal that complexes could bind to CT-DNA through groove binding. The anti-fungal and antibacterial activity against both Gram +ve and Gram –ve bacterial species have been carried out. All the tested complexes showed good antibacterial activity compare to the standard. The antioxidant potential of the compounds was examined by DPPH radical scavenging assay. All the mixed ligand complexes showed promising antioxidant activity than the free ligand. The docking studies have been carried out to find the structure and the mode of binding of complexes with DNA strands. On comparing the docking results, the complexes containing aminotriazole (Atz) have slightly more negative values, indicating that they are more potential DNA binder than the complexes containing aminothiazole (Ath) ligand.

**Acknowledgements** We express our sincere thanks to the Chairman, Department of chemistry, Sahyadri Science College, Kuvempu University for providing laboratory facilities. The authors are thankful to the Indian institute of science and one of the authors thankful to UGC-SAP, phase-III, New Delhi, India.

## References

1. A.A. Khan, K. Iftikhar, *Polyhedron* **13**(23), 3199 (1994)
2. S. Andotra, N. Kalgotra, S.K. Pandey, *Bioinorg. Chem. Appl.* (2014). <https://doi.org/10.1155/2014/780631>
3. I.L. Fedushkin, A.N. Lukoyanov, E.V. Baranov, *Inorg. Chem.* **57**(8), 4301 (2018)
4. P.G. Avaji, B.N. Reddy, S.A. Patil, *Transition Met. Chem.* **31**, 842 (2006)
5. T.S. Kamatchi, N. Chitrapriya, H. Lee, C.F. Fronczek, F.R. Fronczek, K. Natarajan, *Dalton Trans.* **41**, 2066–2077 (2012)
6. M. Becht, T. Gerfin, K.H. Dahmen, *Chem. Mater.* **5**, 137 (1993)
7. M. Pan, G.Y. Meng, H.W. Xin, C.S. Chen, D.K. Peng, Y.S. Lin, *Thin Solid Films* **324**, 89 (1998)
8. P. Dröse, J. Gottfriedsen, *Z. Anorg. Allg. Chem.* **634**, 87 (2008)
9. P. Dröse, J. Gottfriedsen, C.G. Hrib, P.G. Jones, F.T. Edelman, *Z. Anorg. Allg. Chem.* **637**, 369 (2011)
10. J. Jiang, D.K.P. Ng, *Acc. Chem. Res.* **42**, 79 (2009)
11. Y. Bian, J. Jiang, Y. Tao, M.T.M. Choi, R. Li, A.C.H. Ng, P. Zhu, N. Pan, X. Sun, D.P. Arnold, Z.-Y. Zhou, H.-W. Li, T.C.W. Mak, D.K.P. Ng, *J. Am. Chem. Soc.* **125**, 12257 (2003)
12. S.S. Borges, C.U. Davanzo, E.E. Castellano, J.Z. Schpector, S.C. Silva, D.W. Franco, *Inorg. Chem.* **37**(11), 2670 (1998)
13. G.F. Caramori, in *Croatica Chemica Acta*, vol 82, no 1 (Fachbereich Chemie, Philipps-Universität Marburg, Hans-Meerwein-Strasse, D-35032, Marburg, Germany, 2009)
14. D.J. Barnes, R.L. Chapman, R.S. Vagg, E.C. Watton, *J. Chem. Eng. Data* **23**, 349 (1978)
15. N. Venugopal, G. Krishnamurthy, H.S. Bhojyanaik, M. Giridhar, *J. Mol. Struct.* **1191**, 85–94 (2019)
16. N. Venugopal, G. Krishnamurthy, H.S. Bhojyanaik, J.D. Manohara, *J. Inorg. Organomet. Polym.* (2019). <https://doi.org/10.1007/s10904-019-01394-8>
17. H.A. El-Boraey, M.A. El-Salamony, *J. Inorg. Organomet. Polym.* **29**, 684–700 (2019)
18. N. Venugopal, G. Krishnamurthy, H.S. Bhojyanaik, P.M. Krishna, *J. Mol. Struct.* **1183**, 37–51 (2019)
19. M.M. Ibrahim, A.E.M. Ramadan, S.Y. Shaban, G.A.M. Mersal, M.M. Soliman, S. Al-Juaid, *J. Inorg. Organomet. Polym.* **27**, 1252–1263 (2017)
20. D. Mustard, D.W. Ritchie, Docking essential dynamics eigenstructures. *Proteins Struct. Funct. Bioinf.* **60**, 269–274 (2005)
21. B.S. Patil, G. Krishnamurthy, H.S. Bhojya Naik, P.R. Latthe, M. Ghate. *Eur. J. Med. Chem.* **45**, 3329–3334 (2010)
22. G.P.R. Dharsini, C. Thanaraj, R. Velladurai, *J. Inorg. Organomet. Polym.* (2020). <https://doi.org/10.1007/s10904-019-01413-8>
23. D.N. Sathyanarayana, *Electronic Absorption Spectroscopy and Related Techniques* (Universities Press, Hyderabad, 2001)
24. G. Venkatachalam, R. Ramesh, *Spectrochim. Acta A* **61**, 2081 (2005)
25. I.P. Ejidike, P.A. Ajibade, Synthesis, characterization, in vitro antioxidant and anticancer studies of ruthenium (III) complexes of symmetric and asymmetric tetradentate Schiff bases. *J. Coord. Chem.* **68**, 2552 (2015)
26. S. Kumar, G. Krishnamurthy, Y.D. Bodke, V.H. Malojirao, T.R. RN, S. Kandagalla, B.T. Prabhakar, *New J. Chem.* (2018). <https://doi.org/10.1039/C8NJ03057J>
27. G. Krishnamurthy, N. Shashikala, *J. Serb. Chem. Soc.* **74**(10), 1085 (2009)
28. T. Manjuraj, G. Krishnamurthy, Y.D. Bodke, H.S. Bhojya Naik, *J. Mol. Struct.* **1148**, 231 (2017)
29. M.R. Lokesh, G. Krishnamurthy, H.S. Bhojya Naik, N.D. Shashikumar, P. Murali Krishna, *Int. J. Chem. Technol. Res.* **6**, 150 (2014)
30. B. Sreekanth, G. Krishnamurthy, H.S. Bhojya Naik, M.C. Prabhakara, T.K. Vishnuvardhan, *Synth. React. Inorg. Met-Org. Nano-Met. Chem.* **40**, 962 (2010)
31. B.S. Patil, G. Krishnamurthy, H.S. Bhojya Naik, R.L. Prashanth, G. Manjunath, *Eur. J. Med Chem.* **45**, 3329 (2010)
32. B. Sreekanth, G. Krishnamurthy, H.S. Bhojya Naik, T.K. Vishnuvardhana, N. Sharath, B. Vinaykumar, *Nucleosides Nucleotides Nucleic Acids* **30**, 83 (2011)
33. F.A. Saad, H.A. El-Ghamry, M.A. Kassem, A.M. Khedr, *J. Inorg. Organomet. Polym.* **29**, 1337–1348 (2019)
34. P. Lu, M.L. Zhu, P. Yang, *J. Inorg. Biochem.* **95**, 36 (2003)
35. M.Y. Nassar, H.M. Aly, M.E. Moustafa, E.A. Abdelrahman, *J. Inorg. Organomet. Polym.* **27**, 1220–1233 (2017)
36. J.R. Lakowicz, *Principles of Fluorescence Spectroscopy*, 3rd edn. (Springer Publications, New York, 2006)
37. C.V. Kumar, E.H.A. Punzalan, W.B. Tan, *Tetrahedron* **56**, 7027 (2000)
38. P. Kalaiivani, R. Prabhakaran, M.V. Kaveri, R. Huang, R.J. Staples, K. Natarajan, *Inorg. Chim. Acta.* **405**, 415 (2013)

**Publisher's Note** Springer Nature remains neutral with regard to jurisdictional claims in published maps and institutional affiliations.